Journal of Translational Medicine

RESEARCH

Open Access

SLC25A mitochondrial carriers as biomarkers and therapeutic targets of spaceflight-induced dysfunction: the ADP/ATP carrier (AAC3) as a structural case study

Pietro D'Addabbo[1†], Anna De Grassi[1†], Danila Imperia De Luca[1], Valeria Scaglione[1], Anna Lucia Francavilla[1], Sabino Todisco[1], Maria Noemi Sgobba[1], Lorenzo Guerra[1], Mariateresa Volpicella[1], Afshin Beheshti[2,3*] and Ciro Leonardo Pierri[4*]

Abstract

Background Spaceflight exposes living organisms to mechanical unloading and cosmic radiation that profoundly reshape metabolism and tissue function. Because mitochondria play a crucial role in dealing with stress responses, members of the SLC25A carrier family become crucial checkpoints for controlling cellular energy and redox homeostasis.

Methods In this study, we examined the expression of 53 *SLC25A* genes across osteocytes, human bone marrow-derived mesenchymal stem cells (hBMSCs), and mouse brain under microgravity, using curated transcriptomic datasets from NASAs Open Science Data Repository (OSDR). In addition, given that ADP/ATP carriers (AACs) are key mediators of apoptosis, we further investigated AACs through structural modeling and molecular docking with the specific pro-apoptotic (carboxyatractyloside) and anti-apoptotic (bongkrekic acid) inhibitors, with the aim of proposing them as potential targets for apoptosis regulation.

Results Our analysis reveals distinct, tissue-specific expression patterns, with bone cells showing early alteration of the expression of mitochondrial transporters, with enhanced levels of AAC4, CFNc, GC1, CIC, and PNC2, together with reduced UCP2, OGC, and AGC2. These alterations indicate an impaired metabolite transport and gradual metabolic adaptation. hBMSCs, by contrast, repressed AGC1, CAC, UCP6, ORC1, and GlyC, while increasing AAC3, MFRN1, and *SLC25A40* expression, consistently with weaker oxidative phosphorylation and limited renewal potential. Brain tissue appeared comparatively resilient, displaying only a selective rise in DIC, most likely reflecting adaptive activation of dicarboxylate flux. Structural modeling of AACs highlighted conserved conformational features that can be exploited

†Pietro D'Addabbo and Anna De Grassi equally contributed as first authors.

*Correspondence:
Afshin Beheshti
beheshti@pitt.edu
Ciro Leonardo Pierri
ciro.pierri@uniba.it

Full list of author information is available at the end of the article

for the structural modeling of all mitochondrial carriers, thereby providing a foundation for the design of drugs targeting all members of the SLC25A family and for the development of selective modulators capable of restoring apoptosis control and mitochondrial function during exposure to microgravity or cosmic radiation.

Conclusions The presented results establish SLC25A carriers as biomarkers and potential therapeutic targets for counteracting bone/muscle loss, mitochondrial dysfunction, and neurodegeneration under space conditions. By integrating transcriptomic analysis with structural modeling, this work provides translational relevance for astronaut health and offers mechanistic insights applicable to terrestrial mitochondrial disorders as well.

Keywords Spaceflight, Microgravity, SLC25A mitochondrial carriers, Gene Set Enrichment Analysis (GSEA), Mitochondrial metabolism, Osteocytes, Bone marrow stem cells (hBMSC), Brain, Oxidative phosphorylation, Cellular adaptation, MitoCarta, MSigDB hallmarks

Introduction

Mitochondria are central organelles in eukaryotic cells that play a critical role in energy metabolism, biosynthesis, and signaling. The SLC25A family of mitochondrial carriers is a group of membrane transporters responsible for the exchange of metabolites, nucleotides, and cofactors across the inner mitochondrial membrane [1–3]. These carriers are essential for maintaining cellular homeostasis and viability, as they couple the flow of metabolites between mitochondria and cytosol [4] with oxidative phosphorylation (OXPHOS) [5, 6], the Krebs cycle, and associated respiratory-chain activities [1–3, 7, 8]. In this way, they sustain the export of ATP generated in the mitochondrial matrix by ATP-synthase, while simultaneously providing precursors for biosynthetic reactions and redox balance in the cytosol [1–3]. Beyond their role as simple transporters, SLC25A carriers serve as dynamic regulators of mitochondrial bioenergetics and intercompartmental communication [1–3]. They integrate multiple metabolic circuits, including the malate–aspartate shuttle (mediated by the malte/2-oxoglutarate carrier, coded by *SLC25A11* and Asp/Glu carriers, coded by *SLC25A12* or *SLC25A13* [9, 10]), which equilibrates cytosolic and mitochondrial NADH/NAD^+ pools; the citrate/isocitrate–malate shuttle (driven by *SLC25A1 and SLC25A11*), which connects mitochondrial acetyl-CoA export to lipid and cholesterol synthesis [11]; and the carnitine/acylcarnitine shuttle (driven by *SLC25A20*), which coordinates fatty acid β-oxidation with cytosolic lipid turnover [12]. Other carriers, such as the ornithine carrier (*SLC25A15*), participate in the urea cycle and amino acid metabolism [13], while phosphate (*SLC25A3*) and dicarboxylate (*SLC25A10*) carriers [14] maintain the provision of substrates and cofactors to the electron transport chain [15, 16]. Through these tightly coordinated exchanges, SLC25A members act as gatekeepers of cellular metabolic flexibility, enabling mitochondria to adjust energy output and biosynthetic fluxes to varying physiological or environmental demands. From an evolutionary perspective, mitochondrial carriers represent one of the most ancient and conserved protein families in eukaryotes [4, 17]. Comparative genomic and structural analyses indicate that the core SLC25A scaffold emerged early during eukaryogenesis, co-evolving with the respiratory-chain complexes and the oxidative phosphorylation (OXPHOS) machinery to optimize chemiosmotic coupling and metabolite exchange [5, 17–19]. This co-evolution established the tight energetic and metabolic integration between substrate transport, electron flow, and ATP synthesis that sustain eukaryotic bioenergetics. The persistence of these transport systems across plants, fungi, and protists [4, 17, 20–22] underscores their adaptive importance: in these organisms, carrier-mediated exchange sustains metabolic continuity and redox balance even under extreme environmental pressures such as hypoxia, nutrient limitation, high salinity, or radiation exposure. In these microorganisms and life-conditions, the metabolite transport system ensures metabolic continuity and redox stability, highlighting how evolutionary optimization of SLC25A function underlies adaptive resilience across diverse life forms [4, 17, 20–22]. These conserved principles of mitochondrial exchange appear thus relevant under spaceflight conditions, where microgravity and cosmic radiation impose energetic and oxidative stress similar to those encountered in other extreme environments.

Remarkably, dysfunctions in the human SLC25A carriers have been implicated in a variety of human diseases, including cancer, metabolic syndromes, and inherited mitochondrial disorders [23, 24].

Among these transporters, the ADP/ATP carrier is particularly noteworthy because, beyond its role in OXPHOS manintenace, it is also involved in the the assembly of the permeability transition pore (PTP), a critical regulator of apoptosis [25]. Other SLC25A carriers, such as the aspartate-glutamate carriers [9, 10], are similarly important, contributing to processes like myelination, neurodevelopment, and inflammation [11, 26–28].

Spaceflight conditions, including microgravity and space radiation, impose unique stresses on biological systems [29, 30]. These conditions are known to affect

Table 1 Mitochondrial carriers of the SLC25A family

Gene name and NCBI gene link	Human Gene Locus	Transcript (or PseudoGene) Accession ID main isoform (often called isoforn a)/ [other isoforms]	Protein name	alias	Main substrates observed in functional/characterization assays	Related literature	Characterization assay	Tissue distribution	Link to pathological mutations and associated diseases
SLC25A1	12q23	NM_005888	citrate carrier	CIC (CTP)	citrate, malate	[26, 42]	transport assays	liver, kidney, pancreas (also brain, lung, heart)	https://www.hgmd.cf.ac.uk/ac/gene.php?gene=SLC25A1
SLC25A2	5q31	NM_031947	ornithine carrier	ORC2	asymmetric dimethyl arginine, basic amino acids	[43]	transport assays	liver, testis, spleen, lung, pancreas, small intestine, brain, kidney	http://www.hgmd.cf.ac.uk/ac/gene.php?gene=SLC25A2
SLC25A3	12q23	NM_005888 [NM_002635] [NM_213611]	phosphate carrier	PHC (PiC)	phosphate, H+	[44]	transport assays	heart, skeletal muscle and diaphragm [liver, brain, thymus, lung, heart, skeletal muscle, diaphragm]	http://www.hgmd.cf.ac.uk/ac/gene.php?gene=SLC25A3
SLC25A4	4q35	NM_001151	ADP/ATP carrier 1	AAC1, ANT1	ADP, ATP	[45, 46]	transport assays	heart, skeletal muscle, much less in brain, pancreas,kidney, lung, thymus	http://www.hgmd.cf.ac.uk/ac/gene.php?gene=SLC25A4
SLC25A5 [SLC25A5P1]	Xq24-Xq26 [22q13.2]	NM_001152 [NG_009276]	ADP/ATP carrier 2	AAC2, ANT2	ADP, ATP	[25]	transport assays	brain, lung, kidney, pancreas, heart, skeletal muscle, spleen	https://www.hgmd.cf.ac.uk/ac/gene.php?gene=SLC25A5
SLC25A6 [*SLC25A6P1*]	Xp22.32, Yp11.3 [20p11.22]	NM_001636 [NG_003107]	ADP/ATP carrier 3	AAC3, ANT3	ADP, ATP	[47]	Isothermal titration calorimetry	brain, lung, kidney, liver, pancreas, heart, skeletal muscle, spleen, thymus	https://www.hgmd.cf.ac.uk/ac/gene.php?gene=SLC25A6
SLC25A7	4q28-q31	NM_021833	uncoupling protein 1	UCP1	H+	[48]	cell-based assays	brown adipose tissue	https://www.hgmd.cf.ac.uk/ac/gene.php?gene=UCP1
SLC25A8	11q13	NM_003355	uncoupling protein 2	UCP2	(C4 metabolites) Aspartate/Dicarboxylates/Sulfate/Pi	[49]	transport assays	brain, lung, kidney, spleen, hert	https://www.hgmd.cf.ac.uk/ac/gene.php?gene=UCP2
SLC25A9	11q13	NM_003356 [NM_022803]	uncoupling protein 3	UCP3	(C4 metabolites) Aspartate/Dicarboxylates/Sulfate/Pi	[50]	transport assays	skeletal muscle	https://www.hgmd.cf.ac.uk/ac/gene.php?gene=UCP3
SLC25A10	17q25.3	NM_012140	dicarboxylates carrier	DIC	dicarboxylates, phosphate	[14]	transport assays	liver, kidney, heart, brain, lung, pancreas	https://www.hgmd.cf.ac.uk/ac/gene.php?gene=SLC25A10
SLC25A11	17p13.3	NM_003562	malate/oxoglutarate carrier	OGC	malate, 2-oxoglutarate	[51]	transport assays	heart, skeletal muscle, liver, kidney, brain, pancreas	https://www.hgmd.cf.ac.uk/ac/gene.php?gene=SLC25A11
SLC25A12	2q24	NM_003705	aspartate/glutamate carrier 1	AGC1	aspartate, glutamate	[25, 52]	transport assays	brain, heart, skeletal muscle lung, pancreas, kidne (but not in liver)	https://www.hgmd.cf.ac.uk/ac/gene.php?gene=SLC25A12
SLC25A13	7q21.3	NM_014251	aspartate glutamate carrier 2	AGC2	aspartate, glutamate	[25, 52–54]	transport assays, isothermal titration calorimetry	liver, kidney, pancreas, heart, skeletal muscle, brain	https://www.hgmd.cf.ac.uk/ac/gene.php?gene=SLC25A13
SLC25A14	Xq24	NM_003951 [NM_022810]	uncoupling protein 5	UCP5	SO_4^{2-}/Pi/Mal (other dicarboxylates)	[55]	transport assays	widely expressed with highest levels in brain and testis	https://www.malacards.org/search/results?q=SLC25A14
SLC25A15 [*SLC25A15P1*]	13q14.11 [Yq11.223]	NM_014252 [NG_002817]	ornithine carrier 1	ORC1	ornithine, basic aminoacids	[13, 25, 56]	transport assays	liver, pancreas, testis, small intestin, spleen, kidney, brain, heart	https://www.hgmd.cf.ac.uk/ac/gene.php?gene=SLC25A15
SLC25A16	10q21.3	NM_152707	grave's disease carrier	GDC	CoA metabolism (?)	[57]	cell-based assays	liver, kidney, thyroid, lung, heart, skeletal muscle, brain	https://www.hgmd.cf.ac.uk/ac/gene.php?gene=SLC25A16
SLC25A17	22q13.2	NM_006358	peroxisomal cofactor carrier	PMP34	NAD/FAD/CoA Peroxisome	[58, 59]	transport assays	brain, kidney, lung, heart, liver, pancreas	https://www.hgmd.cf.ac.uk/ac/gene.php?gene=SLC25A17
SLC25A18	22q11.2	NM_031481	glutamate carrier 2	GC2	glutamate, H+	[60]	transport assays	brain, testis, heart, pancreas, kidney, lung	https://www.hgmd.cf.ac.uk/ac/gene.php?gene=SLC25A18
SLC25A19	17q25.3	NM_021734 [NM_001126122] [NM_001126121]	thiamine-pyrophosphate carrier	TPC, DNC	thiamine-pyrophosphate carrier	[61]	transport assays	brain, testis, lung, kidney, liver, spleen, skeletal muscle, heart	https://www.hgmd.cf.ac.uk/ac/gene.php?gene=SLC25A19

Table 1 (continued)

Gene name and NCBI gene link	Human Gene Locus	Transcript (or PseudoGene) Accession ID main isoform (often called isoform a)/ [other isoforms]	Protein name	alias	Main substrates observed in functional/characterization assays	Related literature	Characterization assay	Tissue distribution	Link to pathological mutations and associated diseases
SLC25A20 [*SLC25A20P1*]	3p21.31 [6p12]	NM_000387 [NG_001087]	carnitine carrier	CAC [CACTP]	carnitine, acylcarnitine	[12]	transport assays	heart, skeletal muscle, liver (also in lung, kidney, brain, placenta)	https://www.hgmd.cf.ac.uk/ac/gene.php?gene=SLC25A20
SLC25A21	14q11.2	NM_030631	2-oxoadipate carrier	ODC	2-oxoadipate, 2-oxoglutarate	[62]	transport assays	kidney, gall bladder, colon, liver, placenta, testis, lung, spleen, skeletal muscle, brain heart	https://www.hgmd.cf.ac.uk/ac/gene.php?gene=SLC25A21
SLC25A22	11p15.5	NM_024698	glutamate carrier 1	GC1	glutamate, H+	[60]	transport assays	pancreas, brain, liver, testis, spleen, kidney, heart, lung, small intestine, pancreatic beta cells	https://www.hgmd.cf.ac.uk/ac/gene.php?gene=SLC25A22
SLC25A23	19p13.3	NM_024103	ATP-Mg/Pi carrier	APC2	ATP-Mg, Pi, ADP, ATP	[63]	transport assays	kidney, lung, small intestine, pancreas, brain, liver, skeletal muscle, heart	https://www.hgmd.cf.ac.uk/ac/gene.php?gene=SLC25A23
SLC25A24	1p13.3	NM_013386 [NM_213651]	ATP-Mg/Pi carrier	APC1	ATP-Mg, Pi, ADP, ATP	[25, 63]	transport assays	testis	https://www.hgmd.cf.ac.uk/ac/gene.php?gene=SLC25A24
SLC25A25	9q34.11	NM_052901 [NM_001006641] [NM_001006642] [NM_001006643]	ATP-Mg/Pi carrier	APC3	ATP-Mg, Pi, ADP, ATP	[63]	transport assays	brain, heart, skeletal muscle, liver, small intestine, lung, pancreas, testis	https://www.hgmd.cf.ac.uk/ac/gene.php?gene=SLC25A25
SLC25A26	3p14.1	NM_173471	S-adenosyl methionine carrier	SAMC	S-adenosyl methionine, S-adenosyl homocysteine	[64]	transport assays	ubiquitous (testis)	https://www.hgmd.cf.ac.uk/ac/gene.php?gene=SLC25A26
SLC25A27	6p11.2-q12	NM_004277	uncoupling protein 4	UCP4	aspartate, other C4 metabolites	[2, 65]	prediction-based/closest homolog in other organisms, transport assays	brain	https://www.malacards.org/search/results?q=SLC25A27
SLC25A28	10q23-q24	NM_031212	mitoferrin-2	MFRN2	Iron Uptake (FeS clusters)	[66]	cell-based assays	ubiquitous (heart, liver, kidney)	https://www.malacards.org/search/results?q=SLC25A28
SLC25A29	14q32.2	NM_001039355	basic aminoacid carrier	C14orf69, CACL, ORNT3	basic amino acids (arginine, lysine, to a lesser extent ornithine)	[67]	transport assays	heart, skeletal muscle, liver, brain	https://www.hgmd.cf.ac.uk/ac/gene.php?gene=SLC25A29
SLC25A30	13q14.12	NM_001010875	Kidney mitochondrial carrier protein (uncoupling protein 6)	KMCP (UCP6)	SO_4^{2-}/Pi/Mal (other dicarboxylates)	[55]	transport assays	kidney	https://www.hgmd.cf.ac.uk/ac/gene.php?gene=SLC25A30
SLC25A31	4q28.1	NM_031291	ADP/ATP carrier 4	AAC4, ANT4	ADP, ATP	[68]	transport assays	tests	https://www.hgmd.cf.ac.uk/ac/gene.php?gene=SLC25A31
SLC25A32	8q22.3	NM_030780	mitochondrial folate carrier	MFT	Folate/FAD	[69, 70]	cell-based assays	Liver, urinary bladder, lymph node	https://www.hgmd.cf.ac.uk/ac/gene.php?gene=SLC25A32
SLC25A33	1p36.22	NM_032315	Pyrimidin carrier 1	PNC1	uracil, thymine, and cytosine (deoxy)nucleoside di- and triphosphates, guanine nucleotides by antiport	[71]	transport assays	ubiquitous	https://www.malacards.org/search/results?q=SLC25A33
SLC25A34	1p36.21	NM_207348	NA	NA	organic acid, structurally related to yeast OAC1p	[2, 72]	prediction-based/closest homolog in other organisms, transport assays on homologous carriers from other organisms	Skeletal muscle, heart, tongue	NA

Table 1 (continued)

Gene name and NCBI gene link	Human Gene Locus	Transcript (or PseudoGene) Accession ID main isoform (often called isoform a)/ [other isoforms]	Protein name	alias	Main substrates observed in functional/characterization assays	Related literature	Characterization assay	Tissue distribution	Link to pathological mutations and associated diseases
SLC25A35	17p13.1	NM_201520	NA	NA	organic acid, structurally related to yeast OAC1p	[2,72]	prediction-based	Testis, kidney	https://www.malacards.org/search/results?q=SLC25A35
SLC25A36	3q23	NM_018155 [NM_001104647]	Pyrimidin carrier 2	PNC2	cytosine and uracil (deoxy)nucleoside mono-, di-, and triphosphates and guanine nucleotides by uniport and antiport	[71]	transport assays	Ubiquitous	https://www.hgmd.cf.ac.uk/ac/gene.php?gene=SLC25A36
SLC25A37	8p21.2	NM_016612	mitoferrin-1	MFRN1	Iron Uptake (FeS clusters)	[73]	cell-based assays	spleen, placenta	https://www.malacards.org/search/results?q=SLC25A37
SLC25A38	3p22.1	NM_017875	NA	GlyC	gly/ser	[74]	transport assays	Erythroid?	https://www.hgmd.cf.ac.uk/ac/gene.php?gene=SLC25A38
SLC25A39	17q12	NM_016016 [NM_001143780]	NA	CGI69	glutathione/FeS clusters	[75, 76]	cell-based assays	Ubiquitous	https://www.hgmd.cf.ac.uk/ac/gene.php?gene=SLC25A3
SLC25A40	7q21.12	NM_018843	NA	MCFP	glutathione/FeS clusters (A39 seq/structure related)	[2]	prediction-based	Ubiquitous	https://www.hgmd.cf.ac.uk/ac/gene.php?gene=SLC25A40
SLC25A41	19p13.3	NM_173637	ATP-Mg/Pi carrier	APC4	ATP-Mg/Pi	[2]	prediction-based	Liver, testis, brain	https://www.hgmd.cf.ac.uk/ac/gene.php?gene=SLC25A41
SLC25A42	19p13.11	NM_178526	CoA/PAP carrier	CoAPC	CoA, PAP/dPCoA in structurally related closest homolg in other organisms	[77, 78]	transport assays	Ubiquitous (adipose tissue)	https://www.hgmd.cf.ac.uk/ac/gene.php?gene=SLC25A42
SLC25A43	Xq24	NM_145305	NA	NA	nucleotides	[2]	prediction-based	Adrenal gland, skeletal muscle	https://www.hgmd.cf.ac.uk/ac/gene.php?gene=SLC25A43
SLC25A44	1q22	NM_014655 [NM_001135672]	NA	NA	NA	[79]	Bioinformatics and Polymorphism Analysis, transport assays	Liver, kidney, brain	https://www.hgmd.cf.ac.uk/ac/gene.php?gene=SLC25A44
SLC25A45	11q13.1	NM_182556 [NM_001077241]	NA	NA	carnitine like substrates, amino acids	[2]	prediction-based	Skeletal muscle, intestine	https://www.hgmd.cf.ac.uk/ac/gene.php?gene=SLC25A45
SLC25A46	5q22.1	NM_138773	NA	NA	NA?	[80]	cell-based assays	Skeletal muscle	https://www.hgmd.cf.ac.uk/ac/gene.php?gene=SLC25A46
SLC25A47	14q32.2	NM_207117.4	NA	C14orf68, HDMCP	amino acids	[2, 81]	prediction-based/cell-based	Liver	https://www.hgmd.cf.ac.uk/ac/gene.php?gene=SLC25A47
SLC25A48	5q31.1	NM_145282.5	NA	NA	choline	[82]	cell-based	Brain, kidney	https://www.hgmd.cf.ac.uk/ac/gene.php?gene=SLC25A48
SLC25A49	6p21.2	NM_014341.2	mitochondrial carrier homolog 1	MTCH1	NA	[83]	cell-based	Thyroid, Brain, heart, epididymis	https://www.hgmd.cf.ac.uk/ac/gene.php?gene=SLC25A49
SLC25A50	11p11.2	NM_014342.4	mitochondrial carrier homolog 2	MTCH2	NA	[84]	cell-based	Liver, kidney, skeletal muscle, testis	https://www.malacards.org/search/results?q=MTCH2
SLC25A51	9p13.2-p13.1	NM_033412.4	mitochondrial carrier triple repeat 1	MCART1	NAD+/NADP+?	[85–87]	cell-based	Ubiquitous	https://www.malacards.org/search/results?q=SLC25A51

Table 1 (continued)

Gene name and NCBI gene link	Human Gene Locus	Transcript (or PseudoGene) Accession ID main isoform (often called isoform a)/ [other isoforms]	Protein name	alias	Main substrates observed in functional/characterization assays	Related literature	Characterization assay	Tissue distribution	Link to pathological mutations and associated diseases
SLC25A52	18q12.1	NM_001034172.4	mitochondrial carrier triple repeat 2	MCART2	NA	[85–87]	cell-based	Testis	https://www.malacards.org/search/results?q=SLC25A52
SLC25A53	Xq22.2	NM_001012755.5	mitochondrial carrier triple repeat 6	MCART6	NA	[88]	cell-based	Brain, spleen, thymus, lymph node	https://www.hgmd.cf.ac.uk/ac/gene.php?gene=SLC25A53

Human mitochondrial carriers and their coding genes, transcripts, protein names main translocated substrates, tissue distribution, and reference to HGMD/Malacards database for each gene are reported in the table. All the listed mitochondrial carriers are located within the inner mitochondrial membrane, with the exception of CoA/FAD/NAD+ carrier, coded by SLC25A17, located in the peroxisome membrane, and the uncharacterized mitochondrial carriers MTCH1 and MTCH2 coded by SLC25A49 and SLC25A50, respectively, whose localization between the inner and the outer mitochondrial membrane is still debated

cellular physiology, leading to phenomena such as bone and muscle loss, central nervous system (CNS) dysfunction, and systemic inflammation [31]. Luckily, recent studies have expanded our understanding of biological adaptation and diagnostic strategies in aerospace and biomedical contexts [32]. For instance, it was highlighted the utility of salivary diagnostics for monitoring human performance under simulated flight stress [33]. Based on the new diagnostics tools, the role of mitochondria in mediating these effects has gained increasing attention, particularly given their centrality to metabolic regulation and oxidative stress responses. It has previously been shown that mitochondria dysfunction is the central hub increased health risks in humans caused by the space environment [34, 35], but the specific impact of spaceflight on the expression and function of SLC25A mitochondrial carriers remains poorly understood.

To address this knowledge gap, we screened publicly available datasets from NASAs Open Science Data Repository (OSDR) to examine how spaceflight affects SLC25A protein expression in various tissues [36]. Using osteocyte, bone marrow stem cells, and brain tissue data from mice and humans flown to the International Space Station (ISS), we performed differential expression analyses and pathway enrichment studies to assess the regulation of mitochondrial transporters and their associated pathways. These findings provide insights into the molecular mechanisms underlying spaceflight-induced physiological changes and identify potential targets for mitigating damage caused by microgravity and radiation. In addition, we propose that a subset of SLC25A carriers may act as sentinel biomarkers of mitochondrial stress, enabling predictive diagnostics and pharmacological intervention in both spaceflight-related pathology and terrestrial mitochondrial disease.

Beyond their fundamental role in metabolite exchange, SLC25A carriers are emerging as translationally relevant nodes linking mitochondrial homeostasis with tissue resilience and degeneration [15, 16]. Understanding their regulation mitochondrial adaptations to microgravity, the present analysis provides a conceptual bridge between space biomedicine and clinical mitochondrial research. Identifying specific SLC25A carriers (e.g., AAC3, AGC1/2, DIC) as stress-responsive elements enables their use as biomarkers for monitoring tissue health during long-duration missions and as pharmacological targets to prevent bone resorption, stem-cell exhaustion, and neurodegeneration. These findings may also inspire countermeasures applicable to age-related or metabolic diseases on Earth

Materials and methods

Data sources

Data were obtained from NASAs GeneLab platform [36], a repository for spaceflight omics datasets. Three datasets were selected for analysis:

- **OSD-324** (https://osdr.nasa.gov/bio/repo/data/studies/OSD-324): Osteocytes from mice cultured aboard the ISS for 2, 4, and 6 days.
- **OSD-546** (https://osdr.nasa.gov/bio/repo/data/studies/OSD-546): Human bone marrow stem cells (hBMSC) cultured on the ISS for 14 days.
- **OSD-352** (https://osdr.nasa.gov/bio/repo/data/studies/OSD-352): Brain tissue from mice exposed to 12 weeks (84 days) of spaceflight conditions.

All datasets were retrieved from NASAs Open Science Data Repository (OSDR, 2016–2024) and were selected based on the presence of both spaceflight and matched ground control conditions, and standardized omics preprocessing pipelines. Raw read counts were normalized using the DESeq2 median-of-ratios method. Low-count genes were filtered out (baseMean < 10), and normalized counts were $\log_2$-transformed prior to visualization and downstream enrichment analyses. The different durations reflect the availability and design of the spaceflight missions: short-term (2–14 days) or long-duration (84 days).

Gene expression analysis

Processed differential expression data was obtained from NASAs OSDR site, which provides the processed data files utilizing the standard omics pipelines and workflows that are described on NASAs OSDR Github page: https://github.com/nasa/GeneLab_Data_Processing. The expression profiles of the SLC25A mitochondrial carrier family were extracted from the datasets. A heatmap was generated to visualize changes in gene expression across tissues and experimental conditions.

Pathway enrichment analysis

Gene Set Enrichment Analysis (GSEA) [37] was performed using the R fGSEA package [38] on the differential expression files and the genes were ranked using the "t-score" or "Stat" values. The following curated pathways:

1. **Custom SLC25A Pathway**: A gene list specific to SLC25A mitochondrial carriers (Table 1).
2. **MitoCarta Pathway**: A comprehensive mitochondrial gene inventory from the Broad Institute [39].
3. **MSigDB Hallmark Pathways**: Well-defined biological pathways from the Molecular Signatures Database [40].
4. **Custom Mitochondrial Pathways**: Developed and used in COVID-19 research [41].

The GSEA analysis was conducted using the normalized enrichment score (NES) to determine pathway activation or inhibition. As recommended by the GSEA tutorial, a false discovery rate (FDR) threshold of < 0.25 was applied to identify significant results. In more detail, differentially expressed genes were identified using an adjusted p-value (Benjamini–Hochberg correction) of < 0.05. This cutoff ensured stringent gene-level significance, while subsequent pathway enrichment analyses used the GSEA-recommended FDR < 0.25 threshold for exploratory biological interpretation. Each dataset analyzed included a minimum of three biological replicates per condition, as detailed in GeneLab mission metadata. Statistical validation of differential expression was performed within the DESeq2 framework using Wald tests with Benjamini–Hochberg correction.

3D protein comparative modeling and structural analysis

The ADP/ATP carrier (AAC, coded in *H. sapiens* by *SLC25A4* (AAC1), *SLC25A5* (AAC2), *SLC25A6* (AAC3) and *SLC25A31* (AAC4)) is the best-studied member of the mitochondrial carrier (MC) family and the only one for which multiple high-resolution crystallized structures are available [25, 89–92]. Several AAC structures have been solved in the cytoplasmic-open (c-) conformation, each bound to the inhibitor carboxyatractyloside (CATR), a well-known and potent blocker of the transporter. These include two bovine AAC1 structures (PDB IDs: 1OKC and 2C3E [90]) and four yeast AAC2/3 structures (PDB IDs: 4C9G, 4C9H, 4C9J, and 4C9Q [91]).In contrast, only one structure of AAC has been determined in the matrix-open (*m*-) conformation: the *Thermothelomyces thermophilus* AAC1, crystallized with bongkrekic acid (PDB ID: 6CGI [92]).

As a proof of concept, the human ADP/ATP carrier paralog 3 (AAC3) was modelled in both the cytosolic and matrix conformations. With this aim, the sequences and templates were aligned and processed using SwissPDBViewer (SPDBV) according to our validated 3D modelling protocols [10, 12, 25]. The bovine AAC1 (1OKC.pdb) served as the template for the c-conformation because of its high resolution (2.2 Å) and high sequence similarity with the human carrier (about 90% of identical residues). The *T. thermophilus* AAC1 (6GCI.pdb) was used as the template for the m-conformation; this structure shares roughly 58% identical residues with the human sequence and represents the only available matrix-open state.

Conserved sequence motifs typical of mitochondrial carriers, including the PX[D/E]XX[K/R]X[K/R] and [D/E]GXXXX[W/Y/F][K/R]G signatures, were used to anchor the sequence–structure alignment [2, 10, 12, 25]. During model building, the Cα backbone of the human target was restrained to that of the template, and distance constraints were applied to maintain known salt bridges that stabilize each conformational state [2, 10, 12, 25, 93]. A restrained molecular dynamics optimization with gradual annealing was then carried out to generate a set of 100 trial structures for each conformation [10, 12, 25].

The models were evaluated for overall geometry and energy using the WHAT IF web server, and the structures with the best stereochemical properties were selected for further visual inspection with PyMOL [2, 10, 12, 25, 93]. The root-mean-square deviation (RMSD) between the human models and their corresponding templates was calculated in PyMOL using the "super" command to assess how closely the modeled structures matched the crystallized templates.

Re-docking and docking analysis

To validate the accuracy of the modeled binding cavities of the human ADP/ATP carrier (AAC3) in both conformational states, we performed docking analyses with its two canonical inhibitors: carboxyatractyloside (CATR), which stabilizes the cytoplasmic-open (c-) conformation, and bongkrekic acid (BKA), which locks the protein in the matrix-open (*m*-) conformation. These two ligands have been co-crystallized with the previously mentioned homologous AACs and are well-characterized reference inhibitors for AACs [25, 89].

Prior to the docking simulations, the 3D models of the human AAC3 in c- and m-conformations were converted from ".pdb" to ".pdbqt" format using the MGLTools suite of AutoDock 4.2. Partial charges were assigned to each atom using the Gasteiger method. The ligands CATR and BKA were extracted from their crystallographic complexes (PDB IDs: 1OKC for the *B. taurus* AAC1–CATR complex and 6GCI for the *T. thermophilus* AAC1–BKA complex) and converted to ".pdbqt" format using AutoDock scripts.

To identify the optimal gridbox parameters for each conformation, a series of ten re-docking simulations were performed by varying the size and position of the gridbox to best reproduce the crystallized inhibitor poses within the previously mentioned corresponding crystallized AACs. The final gridbox for the c-conformation (CATR-bound) consisted of $34 \times 34 \times 60$ grid points along the x, y, and z axes, with a spacing of 0.281 Å. The gridbox center was positioned to include residues known to interact with CATR in the bovine AAC1 crystallized structure, aligning with the center of mass of residues R80, G183, R280 in the human AAC3 model in c-conformation. The final gridbox for the m-conformation (BKA-bound) consisted of $26 \times 30 \times 22$ grid points along the x, y, and z axes, with a spacing of 0.281 Å. The gridbox center was located within an equivalent internal cavity in a bit enlarged (along y axis) and shorter (along z axis) gridbox to allow the free bending of BKA in the space. This gridbox includes all the residues of the bottom half of the carrier in m-conformation protruding towards the carrier cavity and aligns with the center of mass of residues R80, G183, R280 in the human AAC3 model in m-conformation.

Either re-docking or docking simulations were executed using the Lamarckian genetic algorithm implemented in AutoDock 4.2. The following parameters were used for both ligands: rmstol = 1.5 Å, ga_pop_size = 50, ga_num_evals = 2.5×10^5, and ga_num_generations = 2.7×10^4. The five top-ranked individuals from each generation were retained for the next iteration, and cluster analyses were conducted on the resulting 50 ligand poses to identify the most representative binding conformations.

The quality of the docking results was assessed by comparing the predicted binding poses with those observed in the native crystallized complexes. Each re-docked/docked complex was superimposed on its experimental counterpart (BtAAC1–CATR or TtAAC1–BKA) using PyMOL, and the root mean square deviation (RMSD) between the heavy atoms of the docked and crystallized ligands was calculated.

Statistical analysis

As RNA-seq data were created from different labs and experiments, each dataset was normalized and processed individually and then the log2(fold-change) values were compared across all datasets. The analyses were performed using R (version 4.3.3) and Python (version 3.12.3) with packages including DESeq2 for differential expression, ComplexHeatmap for visualization, and the GSEA software suite for pathway enrichment. Temporal normalization was not applied across independent mission datasets. Instead, we examined directionality and enrichment coherence across timepoints within each tissue to infer intrinsic versus duration-dependent responses.

Data interpretation

Changes in the SLC25A family expression were correlated with functional pathways to assess their potential roles in bone, brain, and systemic health under spaceflight conditions. Tissue-specific trends were identified, and implications for space-induced damage were discussed in the context of existing literature.

Results and discussion

Expression patterns of SLC25A genes across tissues and conditions

Mitochondrial carriers of the SLC25A (Table 1) family exhibited tissue- and duration-dependent transcriptional responses to spaceflight (Fig. 1). Short-term exposures (2–6 days) captured early adaptive responses in osteocytes and hBMSCs, whereas the 84-day brain dataset provided a window into long-term microgravity adaptation in the central nervous system. A long exposure to space increases both the damage caused by the microgravity environment and the total accumulated dose of high Linear Energy Transfer (LET) space radiation the samples received. In osteocytes, short-term microgravity exposure (2–6 days) was associated with a robust upregulation of genes involved in (i) glutamate exchange/uptake, namely *SLC25A18* and *SLC25A22*, coding for glutamate carrier paralog 2 (GC2) and 1 (GC1), respectively, (ii) fatty acid metabolism, namely *SLC25A17*, coding for the peroxisome CoA/FAD/NAD^+ carrier (CFNC), (iii) nucleotide transport, namely *SLC25A31*, coding for the ADP/ATP carrier paralog 4 (AAC4), and *SLC25A36* coding for pyrimidine carrier paralog 2 (PNC), and (iv) inflammation and tricarboxylic acid cycle, namely *SLC25A1*, coding for citrate carrier (CIC). Concomitantly, a downregulation of key transporters mediating (i) either proton or C4 metabolite exchanges, namely *SLC25A8*, coding for uncoupling protein paralog 2 (UCP2), and (ii) malate/aspartate shuttle, namely *SLC25A13* coding for aspartate/glutamate carrier paralog 2 (AGC2) and *SLC25A11* (OGC), was detected, indicating a coordinated remodeling of mitochondrial metabolite flux during early adaptation to microgravity.

These data point to a rapid and highly plastic adaptation of bone-associated mitochondrial carriers to spaceflight (Fig. 1 and Table 1). The early osteocytic upregulation of *SLC25A1* (CIC) and *SLC25A18* (GC2)/*SLC25A22* (GC1), for example, likely reflects a compensatory response to affected TCA cycle input/output and glutamate metabolism, both of which are essential for redox balance and matrix production. Downregulation of *SLC25A11* (OGC), *SLC25A13* (AGC2), and *SLC25A8* (UCP2)

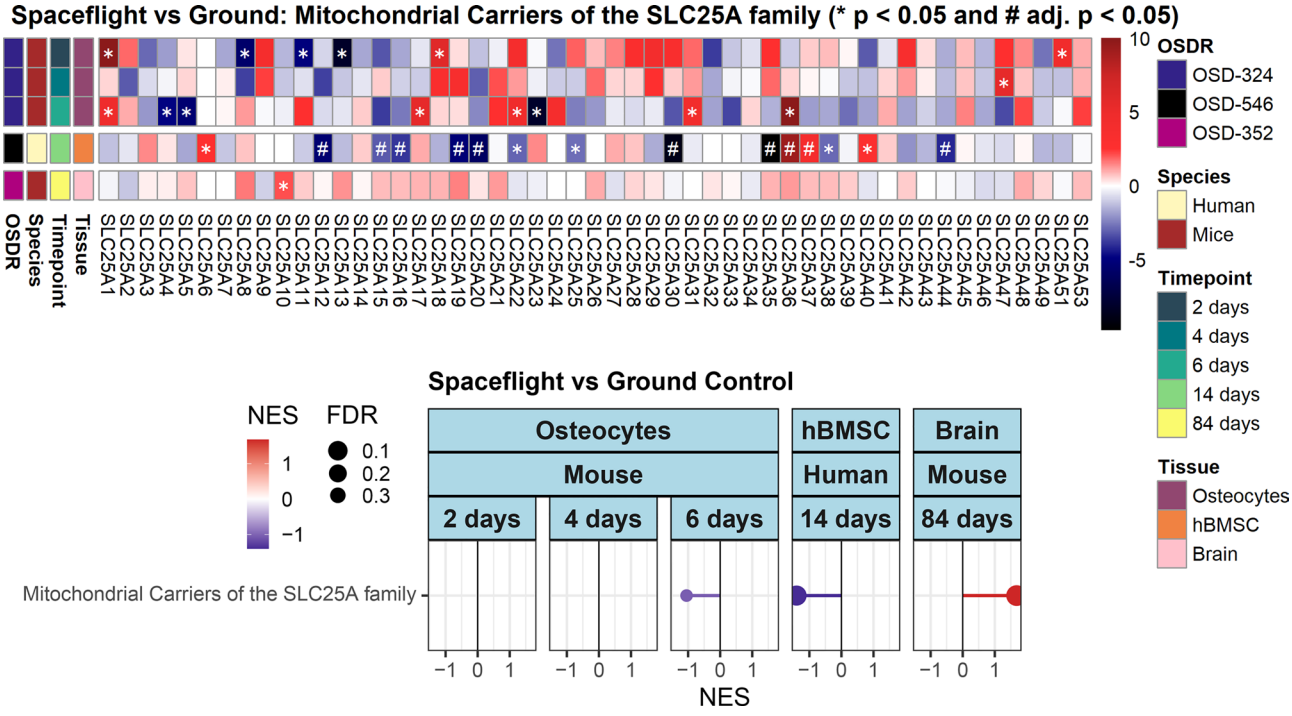

Fig. 1 Transcriptional adaptation of the SLC25A mitochondrial carrier family to spaceflight. Heatmap illustrating normalized enrichment scores (NES) for 53 SLC25A family genes across osteocytes, human bone marrow stem cells (hBMSCs), and brain tissues under spaceflight versus ground control conditions. Each column corresponds to a specific species, tissue, and timepoint (2, 4, 6, 14, or 84 days), across datasets OSD-324, OSD-352, and OSD-546. Rows represent individual SLC25A genes. NES values are color-coded (red, upregulation; blue, downregulation), with statistical significance indicated by asterisks (*$p < 0.05$) or hash marks (# adjusted $p < 0.05$). SLC25A50 and SLC25A52 were not present in the processed data and were filtered out in the quality control stage. Below the heatmap, a gene set enrichment analysis (GSEA) was performed on a custom-defined "SLC25A family" pathway constructed from the listed genes. The lower lollipop plot shows the NES, reflecting pathway activation (positive NES) or inhibition (negative NES), with circle size inversely proportional to the false discovery rate (FDR). While GSEA typically recommends a significance threshold of FDR < 0.25, a slightly relaxed cutoff of FDR < 0.3 was applied to better capture subtle pathway trends under spaceflight conditions. GSEA was performed using the standard protocol (https://www.gsea-msigdb.org/gsea/index.jsp). For clarity, only gene names are shown; the associated protein names and functional annotations are provided in Table 1

supports the hypothesis of impaired malate/aspartate and isocitrate malate shuttle activities [1, 3], which may contribute to metabolic decoupling from the cytosol, an early signature of stress-induced mitochondrial dysfunction. Remarkably, the upregulation of *SLC25A31* (AAC4), normally expressed only in testis, *SLC25A36* (PNC2), and the peroxisome *SLC25A17* (CFNc), may indicate an attempt to counterbalance a possible energy demand (through the enhancement of fatty acid metabolism) and mtDNA loss in microgravity conditions, as a consequence of the stress-induced mitochondrial dysfunction.

In human bone marrow-derived mesenchymal stem cells (hBMSCs), a delayed transcriptional response was observed, characterized by significant upregulation of *SLC25A6*, coding for the ADP/ATP carrier paralog 3 (AAC3), *SLC25A36* (PNC2), *SLC25A37* coding for a transporter known as mitoferrin-1 (MFRN1), and *SLC25A40*, coding for a transporter involved in glutathione/iron-sulfur cluster metabolism, after 14 days of spaceflight, accompanied by the downregulation of multiple metabolite transporters including *SLC25A12*, coding for aspartate/glutamate carrier paralog 1 (AGC1), *SLC25A15*, coding for ornithine carrier (ORC1), *SLC25A16*, coding for a transporter involved in CoA metabolism (GDC), *SLC25A20*, coding for carnitine acylcarnitine carrier (CAC), *SLC25A38*, coding for glycine carrier (GlyC), *SLC25A22*, coding for glutamate carrier (GC1), *SLC25A25*, coding for ATP-Mg/Pi carrier (APC3), and *SLC25A30*, coding for UCP6 (also known as KMCP1) (Fig. 1 and Table 1).

These results suggest a mitochondrial functional reprogramming favouring energy maintenance and metabolic flexibility in the bone marrow compartment. In hBMSCs, the downregulation of carriers involved in CoA metabolism (*SLC25A16*). Thiamine pyrophosphate uptake (*SLC25A19*), and fatty acid metabolism (*SLC25A20*), together with *SLC25A38* (GlyC) suggests profound remodeling of organic acid, lipid and one-carbon metabolism. Also amino acid metabolism appears impaired with the downregulation of urea cycle genes, with reference to ORC1 (*SLC25A15*). mal/asp shuttle, with reference to AGC1 (*SLC25A12*), and GC1 (*SLC25A22*). Upregulation of *SLC25A6* (AAC3), *SLC25A36* (PNC2) and *SLC25A40* (MCFP, a transporter involved in iron-sulfur cluster and glutathione metabolism, linked to redox status, structurally related to *SLC25A39* (CGI69) [75]) points to a compensatory increase in ATP turnover and nucleotide exchange, potentially for nucleic acid biosynthesis, and iron cofactor biogenesis, for attempting to counteract oxidative stress or impaired respiration (Fig. 1 and Table 1).

Conversely, brain tissue exhibited minimal transcriptional changes, with only *SLC25A10* coding for the succinate(malate)/Pi carrier (dicarboxylate carrier, known as DIC) significantly upregulated after prolonged exposure (84 days), implying a relative resilience of neuronal mitochondrial transport to microgravity (Fig. 1 and Table 1).

Gene set enrichment analysis (GSEA) supported these findings, revealing significant activation of the *SLC25A* signature in osteocytes after early spaceflight exposure and in hBMSCs after longer exposure, but no enrichment in brain tissue (Figs. 1 and 2).

The lack of significant changes in most brain mitochondrial carriers, except *SLC25A10* (DIC), which supports complex II-linked respiration, suggests a conserved metabolic profile in neural tissues. This aligns with known CNS resistance to metabolic rewiring, potentially linked to glial buffering and blood–brain barrier protection.

While not reaching statistical significance thresholds (FDR < 0.25), additional trends in the specific gene expression of mitochondrial carriers suggested broader alterations in mitochondrial metabolite transport. These included transient upregulation of (i) *SLC25A9* (UCP3), a close paralog of *SLC25A8* (UCP2), involved in proton and C4 metabolite exchange, (ii) *SLC25A21*, coding for 2-oxoadipate/2-oxoglutarate carrier (ODC), *SLC25A24*, coding for ATP-Mg/Pi carrier paralog 1 (APC1), *SLC25A29*, coding for basic amino acid carrier (previously known as CACL), *SLC25A28* (MFRN2), the closest paralog of *SLC25A37*(MFRN1), and *SLC25A42*, coding for CoA/PAP transporter (CoAPC) (Figs. 1 and 2)) in osteocytes during early timepoints, warranting further investigation. *SLC25A50* and *SLC25A52* were not present in the processed data and were filtered out in the quality control stage.

From a translational standpoint, these results identify the upregulation of *SLC25A6* (AAC3)/*SLC25A31* (AAC4) and *SLC25A36* (PNC2) and the downregulation of *SLC25A12* (AGC1) and *SLC25A13* (AGC2), as candidate biomarkers of early mitochondrial stress in space-exposed bone and stem cell tissues. Importantly, several of these carriers are pharmacologically targetable. For instance, small-molecule modulators of nucleotide transporters could restore ATP/ADP or pyrimidine balance (Figs. 1 and 2), whereas AGC modulators are under investigation in cancer models to regulate the impaired mal/asp shuttle [9, 53]. These targets may form the basis for countermeasures aimed at restoring mitochondrial homeostasis in astronauts or spaceflight models.

Among the uncharacterized carriers, the upregulation of *SLC25A47*, predicted to be an amino acid carrier, and *SLC25A51*, recently proposed to participate in NAD^+ uptake, were observed in osteocytes. Conversely, the downregulation of *SLC25A35*, predicted to translocate oxaloacetate or isopropyl-malate structurally related

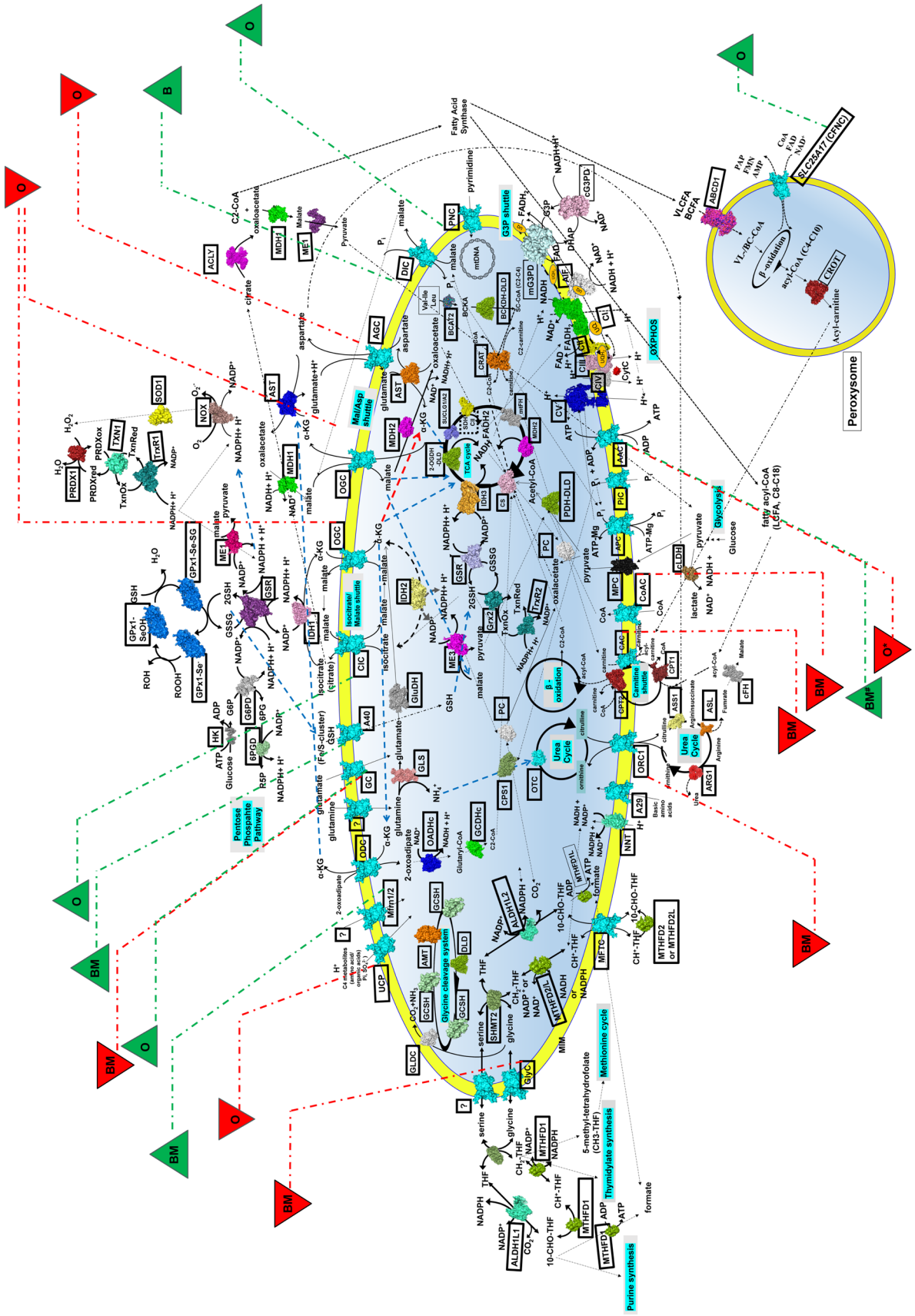

Fig. 2 (See legend on next page.)

(See figure on previous page.)

Fig. 2 Scheme of a mitochondrion with a set of representative characterized mitochondrial transporters of the SLC25A family, and related pathways and cycles. The above reported scheme indicates schematically the main small molecules, cofactors, and proteins interacting more or less directly with the human mitochondrial carriers of the SLC25A protein family. Respiratory chain complexes, mitochondrial transporters, and other proteins are reported in surf representation. Protein labels are reported in black boxes for discriminating them from substrates. ATP synthase (CV) is reported in blue (based on the Bos taurus crystallized structure 6zqn.Pdb). Red/blue/orange transparent circles indicate mitochondrial carriers downregulated/upregulated/rebound-upregulated in microgravity conditions, mitochondrial carriers are reported in cyan (based on the 3D structure of the bovine ADP/ATP carrier, 1okc.Pdb). MPC (an in-house developed 3D comparative model, data not published) is reported in black; PDH in light green (based on the human crystallized structure 6cfo.Pdb); AIF in white (based on the human crystallized structure 4bur.Pdb). Complex I (ci, based on the Ovis aries crystallized structure 5lnk.Pdb), complex ii (CII, based on the Sus scrofa scrofa 3aef.Pdb), complex iii (CIII, based on the O. aries 6q9e.Pdb), and complex IV (CIV) (together with CytC in red, based on the bovine crystallized structure 5iy5.Pdb) are reported in green, yellow, magenta, and grey, respectively. The human isocitrate dehydrogenase 2 (IDH2, pale yellow surface representation in the matrix, based on 6kdf.Pdb), the human isocitrate dehydrogenase 3 (IDH3, orange surface representation in the matrix, based on 6kdf.Pdb), the human isocitrate dehydrogenase 1 (IDH1, pink surface, in the cytosol, based on 1t09.Pdb), the human mitochondrial glutamate dehydrogenase (GluDH, gray surface, in the matrix based on 1l1f.Pdb), the human mitochondrial glutaminase (GLS, salmon surface, based on 6ujm.Pdb), the human nicotinamide nucleotide transhydrogenase (NNT1, light green, inner mitochondrial membrane based on 1u31.Pdb); the human cytosolic lactic dehydrogenase (LDH, yellow-sand color, based on 6baz.Pdb); the human cytosolic (ME1) and matrix (ME3) malic enzyme (colored in brilliant pink and violet, respectively, based on 1pjl.Pdb), the human glutathione reductase (GR, dark magenta surface in the cytosol and light magenta surface in the matrix, based on 1gre,pdb), the human selenocysteine to glycine glutathione peroxidase 4 (GPX4, petroleum blue surface, in the matrix, based on 2gs3.Pdb), the human glucose-6-phosphate dehydrogenase (G6PD, grey surface, based on 5ukw.Pdb), the human superoxide dismutase (SOD1; yellow surface, based on 5ytu.Pdb); the human thioredoxin reductase 1 (TrxR1, dark green surface, based on 2j3n.Pdb); the human thioredoxin (TXN, light green, based on 2ifq.Pdb); the human peroxiredoxin (PRDX1, light brown cartoon, based on 4xcs.Pdb); glycine decarboxylase (GLDC, white cartoon, based on 6i33.Pdb); the human T-protein of glycine cleavage system (amt, white cartoon, based on 1wsv.Pdb); the human H-protein, a lipoamide containing protein of the glycine decarboxylase complex (GCSH, light cyan cartoon, based on 1htpA.Pdb); the human 6-phophogluconate dehydrogenase (6PGD, light green surface, based on 5uq9.Pdb), the human hexokinase (HK, dark grey surface, based on 1hkc.Pdb), the human c/m glycerol-3-phosphate dehydrogenase (m/c-G3PDH, cyan/pink surface, based on 2pla.Pdb), the human cytosolic selenocysteine to glycine mutant of human glutathione peroxidase 1 (GPx1-Se-; Gpx1-SeOH; Gpx1-Se-SG, blue surface, in the cytosol based on 2f8a.Pdb), NADH oxidase (NOX, dark salmon surface representation in the cytosol, based on 8x2l.Pdb), the human serine hydroxy-methyltransferase (SHMT2, green smudge surface representation, based on 8tlc.Pdb), the human methylenetetrahydrofolate dehydrogenase 2 (MTHFD2, green surface representation, based on 7ehj.Pdb), the human 10-formyltetrahydrofolate dehydrogenase (ALDH1L1, light green surface, based on 7rlu.Pdb), the human argininosuccinate synthase (ass, yellow surface, based on 2nz2.Pdb), the human argininosuccinate lyase (ASL, orange surface, based on 1aos.Pdb), the human arginase (ARG1, red surface, based on 6v7d.Pdb), the human ornithine transcarbamylase (OTC, cyan surface, based on 1c9y.Pdb), the human carbamoyl-phosphate synthase (CPS1, smudge surface, based on 5dot.Pdb), the human fumarate hydratase (cFH, for cytosolic, or mtFH, for mitochondrial, both in grey surface, based on 5upp.Pdb), glutaryl-CoA dehydrogenase (GCDHc, green surface, based on 1siq.Pdb), 2-oxoadipate dehydrogenase (OADHc, blue surface, based on 6sy1.Pdb), cytrate synthase (CS, light pink surface, based on 5uzr.Pdb), succynil-CoA synthetase (SUCLG1/A2, slate surface, based on 6g4q.Pdb) are represented by using the PyMOL molecule visualizer. It should be noticed that succinate dehydrogenase participates to respiratory chain (see complex ii, CII) and to the TCA cycle, where it is laabelled by a squared dashed box for recalling its partial localization into the mitochondrial inner membrane. Black circular arrows indicate cyclic pathways. Black solid/dashed lines indicate the possible direction of the reported reactions or metabolite fates. Blue dashed lines indicate reactions involving NADPH or OGC substrates (regarding malate or 2-oxoglutarate). The red dashed line indicates a possible asp/mal shuttle stimulation mediated by an increased uptake of 2-oxoglutarate. Other abbreviations: MIM: mitochondrial inner membrane; UQ, ubiquinone; AAC, ADP/ATP carrier, coded in H. sapiens by SLC25A4 (AAC1), SLC25A5 (AAC2), SLC25A6 (AAC3), SLC25A31 (AAC4); AGC, aspartate/glutamate carrier, coded by SLC25A12 (AGC1) and SLC25A13 (AGC2); DIC, dicarboxylate carrier, coded by SLC25A10; MFTC, assumed to be the FAD (folate/riboflavin) carrier, coded by SLC25A32; OGC, malate/2-oxoglutarate carrier, coded by SLC25A11; CIC, citrate carrier, coded by SLC25A1; PiC, phosphate carrier, coded by SLC25A3; UCP, proton/C4 metabolite carrier coded by SLC25A7_UCP1, SLC25A8_UCP2, SLC25A9_UCP3, SLC25A14_UCP5, SLC25A27 (UCP4), SLC25A30 (UCP6); ODC, 2-oxoadipate/2-oxoglutarate carrier, coded by SLC25A21; APC, ATP-Mg/Pi carrier, coded by SLC25A23 (APC2), SLC25A24 (APC1), SLC25A25 (APC3), SLC25A41 (APC4); ORC1, ornithine carrier, coded by SLC25A15 (ORC1); MFRN, mitoferrin, coded by SLC2537 (MFRN1) or SLC25A28 (MFRN2), respectively. mas, malate/aspartate shuttle reported in an orange transparent box; TCA, tricarboxylic acid cycle; MDH1, cytosolic malate dehydrogenase 1; ME1, malic enzyme 1; MPC, mitochondrial pyruvate carrier; PDH, pyruvate dehydrogenase; CytC, cytochrome C; AIF, apoptosis-inducing factor. "?" indicate uncharacterized mitochondrial carriers. Red dashed lines and red arrow-heads indicate downregulated transporters, whereas green dashed lines and arrow-heads indicate upregulated transporters. "o", "BM", "b" in the arrow-heads indicate osteocytes, hBmscc, or brain, respectively (according to Fig. 1 reported tissues and Table 1). The "*" indicates that SLC25A4 (AAC1), SLC25A5 (AAC2) are downregulated in osteocytes whereas SLC25A31 (AAC4) is upregulated in osteocytes. The "#" indicates that SLC25A6 (AAC3) is upregulated in hBMSC

substrates, due to its phylogenetic relationships with the yeast Oac1p, and *SLC25A44*, predicted to translocate organic acids, was observed in bone marrow.

Pathway-level remodeling of mitochondrial bioenergetics and immune signaling under microgravity

Custom GSEA of mitochondrial and immune pathways (Fig. 3) revealed a second layer of spaceflight-driven adaptation, distinctively shaped by tissue type and duration of exposure to microgravity.

Mitochondrial bioenergetics

In hBMSCs after 14 days of spaceflight, ll OXPHOS-related modules, including respiratory chain assembly factors, complexes I–V, and the mitochondrial ribosome, were significantly downregulated (NES < 0). This repression aligned with the downregulation of amino acid carriers involved in the mal/asp shuttle and reducing equivalents recycle (i.e., *SLC25A12*, AGC1) or urea cycle (i.e., *SLC25A15*, ORC1), depending on the cytosolic aspartate availability, as observed in Fig. 1. By contrast, mouse brain at 84 days exhibited selective upregulation

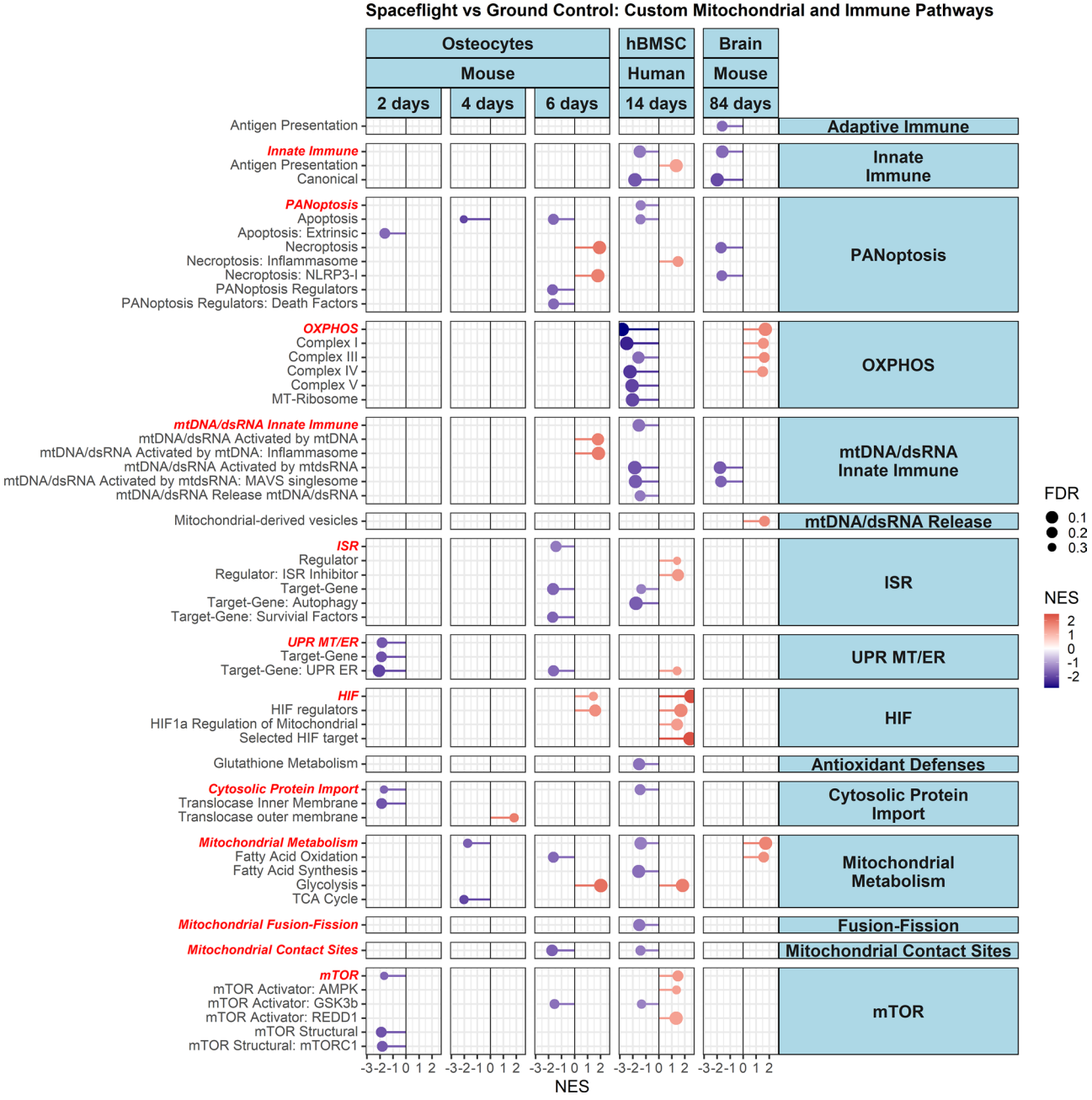

Fig. 3 GSEA of custom mitochondrial and immune pathways in osteocytes, hBMSCs, and brain under spaceflight. ("GSEA-Cust Infl_MITO"): this is a GSEA custom pathway analysis according to [94]. Normalized enrichment scores (NES) for mitochondrial- and immune-related modules (rows) are plotted as lollipops for osteocytes (2, 4, 6 days; mouse), hBMSCs (14 days; human), and brain (84 days; mouse) comparing spaceflight to ground controls. A positive NES indicates pathway activation (red), and a negative NES indicates inhibition (blue). Circle size is inversely proportional to the false discovery rate (FDR); only results with FDR < 0.3 are shown. Pathways were defined in collaboration with D. Wallace [94], and include modules for antigen presentation, innate immunity, PANoptosis (apoptosis, necroptosis, inflammasome), oxidative phosphorylation (OXPHOS) complexes I–V and mitochondrial ribosome, mtDna/dsrna immune sensing and vesicle release, integrated stress response (ISR), unfolded protein response (UPR^MT/ER), hypoxia-inducible factor (HIF) signaling, antioxidant defenses, cytosolic protein import, mitochondrial metabolism (TCA cycle, glycolysis, fatty-acid oxidation/synthesis), fusion–fission dynamics, mitochondrial contact sites, and mTOR network

complexes I, III, and IV (NES > 0), in line with upregulation of the malate/succinate carrier *SLC25A10* (DIC), which supports succinate/malate cycling and respiratory chain. Osteocytes did not display significant OXPHOS enrichment at any early timepoint (Figs. 2 and 3).

The observed OXPHOS repression in hBMSCs is a hallmark of mitochondrial dysfunction and suggests impaired ATP production capacity. The coordinated downregulation of several SLC25A members that shuttle amino acids and organic acids may impair metabolic crosstalk with the cytosol and contribute to reduced stem cell viability or differentiation. Conversely, the brain's compensatory upregulation of *SLC25A10* (DIC), a dicarboxylate transporter, supports enhanced substrate delivery to stimulate electron transport chain, likely a protective adaptation against chronic oxidative stress. These findings highlight the downregulation of *SLC25A12* (AGC1), *SLC25A15* (ORC1) and the upregulation of *SLC25A10* (DIC) as potential biomarkers for energy disruption or resilience in specific tissues and suggest them as pharmacological targets for metabolic support in microgravity (Figs. 2 and 3).

Cell death and proteostasis pathways

Divergent modulation of programmed cell death pathways was observed. Necroptosis (NLRP3 inflammasome) was upregulated in osteocytes at day 6 (NES > 0) but repressed in brain. Interestingly, hBMSCs showed significant upregulation of the inflammasome as a whole pathway (Fig. 3). Intrinsic and extrinsic apoptosis modules were repressed in osteocytes at days 4 and 6, whereas extrinsic apoptosis alone was downregulated at day 2. Remarkably, PANoptosis regulators were downregulated at day 6 in osteocytes, largely due to reduced death-factor transcripts.

The hypoxia-inducible factor (HIF) pathway was robustly induced across hBMSC modules (general modules, regulatory arms, HIF1α, and target genes), with only modest upregulation of the HIF regulator module in osteocytes at day 6 (Fig. 3).

These data reveal a cell-type-specific rewiring of stress responses. The upregulation of inflammasome signaling in hBMSCs and osteocytes (at day 6), and of necroptosis/inflammasome in osteocytes and hBMSCs, may reflect mitochondrial distress due to spaceflight-driven membrane or redox disruption. *SLC25A12* (AGC1)/*SLC25A13* (AGC2) and *SLC25A15* (ORC1), which are involved in amino acid metabolism and redox homeostasis (Table 1, Figs. 2 and 3) and are tightly linked to pro-apoptotic cascades [9, 13], were downregulated in hBMSCs (AGC1 and ORC1, Table 1) and osteocytes (AGC2). This downregulation may reflect reduced mitochondrial activity and justify the observed enhanced necroptosis, driven by increased ROS damage that is normally limited by reducing-equivalent exchange via the malate/aspartate shuttle. The associated shift in cell fate appears to involve both necroptosis and inflammatory signaling, although their causal relationship remains uncertain. This is particularly relevant in light of the mentioned mitochondrial carrier defects linked to neuroinflammation and cell death [23, 24].

The activation of the HIF pathway in osteocytes and hBMSCs aligns with enhanced glycolytic flux and may represent a compensatory response to reduced OXPHOS, mainly observed in hBMSCs. As HIF stabilization promotes survival and angiogenesis under hypoxic stress, targeting upstream carriers or downstream HIF targets could offer avenues for boosting tissue resistance to spaceflight-induced damage.

Immune-signaling modules

Adaptive antigen-presentation pathways (adaptive immune axis) fell significantly in brain at 84 days, whereas innate-immune signaling was uniquely upregulated in hBMSCs (antigen presentation, Fig. 3), but its canonical arm was repressed in both osteocytes (2–6 days) and hBMSCs. MtDNA/dsRNA sensing was strongly inhibited in hBMSCs via mitochondrial antiviral signaling (MAVS) singlesome downregulation, yet despite similar MAVS repression, the brain's mtDNA/dsRNA module remained unchanged, implying compensatory buffering (Fig. 3). Inflammasome activation by mtDNA surged in osteocytes at day 6, whereas mitochondrial-derived vesicle release, a hallmark of organelle quality control, peaked exclusively in brain tissue after 84 days.

The repression of MAVS-linked immune responses in hBMSCs underscores a blunted antiviral and danger-signaling capacity, possibly resulting from impaired mitochondrial dynamics or metabolite depletion most likely related to amino acid carrier downregulation (AGC1, ORC1, GC, GlyC) (Table 1, Figs. 2 and 3). Notably, also carriers involved in organic acid and lipid metabolism (i.e., *SLC25A20* (CAC), *SLC25A30* (UCP6 or KMCP1), and *SLC25A19* (TPC or DNC)) appear downregulated in hBMSCs, suggesting a strong relationship between the correct function of these carriers and immune response. Conversely, the brain's unaltered immune sensing despite MAVS downregulation suggests metabolic or transcriptomic compensation, potentially through other carrier systems like *SLC25A10* (DIC), known for being involved in neurodegeneration [14], or enhanced vesicle trafficking. mtDNA/dsRNA inflammasome activation by mtDNA in osteocytes points to mitochondrial membrane damage or impaired quality control, making vesicle release and SLC25A-linked metabolite accumulation promising indicators of immune stress. Carrier modulation could be used both diagnostically and therapeutically

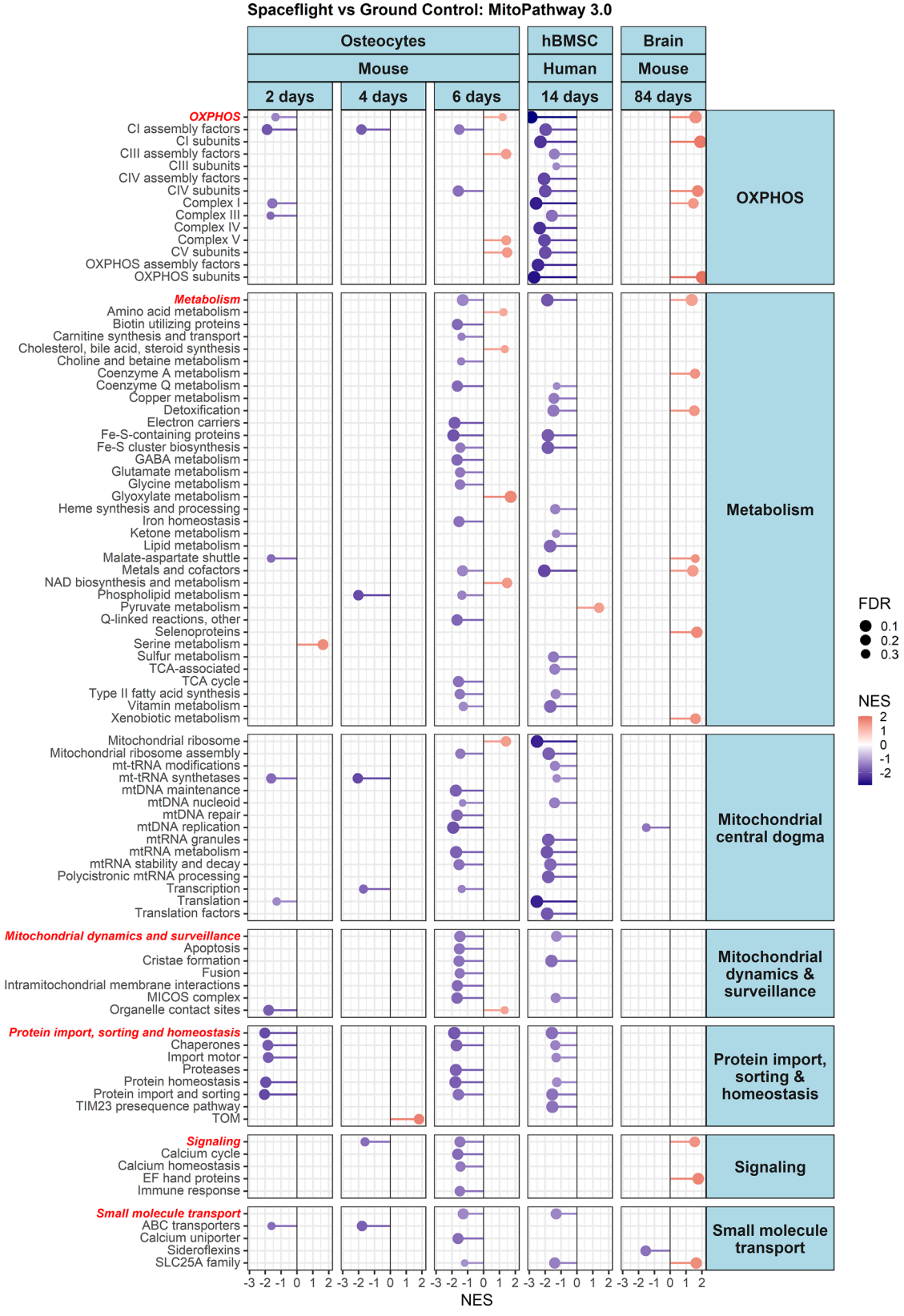

Fig. 4 (See legend on next page.)

(See figure on previous page.)

Fig. 4 GSEA of curated MitoCarta 3.0 ("MitoPathway") modules in osteocytes, hBmscs, and brain under spaceflight [95]. Normalized enrichment scores (NES) for 84 mitochondrial modules (rows), grouped into OXPHOS, metabolism, central dogma, dynamics & surveillance, protein import/sorting/homeostasis, signaling, and small-molecule transport (including SLC25A carriers), are shown as lollipops for mouse osteocytes (2, 4, 6 days), human hBmscs (14 days), and mouse brain (84 days) comparing spaceflight versus ground controls. NES > 0 (red) indicates activation; NES < 0 (blue) indicates inhibition. Circle size is inversely proportional to FDR (only FDR < 0.3 shown). Pathway definitions were obtained from the Broad's MitoCarta 3.0 inventory of mammalian mitochondrial proteins and pathways (https://www.broadinstitute.org/mitocarta/mitocarta30-inventory-mammalian-mitochondrial-proteins-and-pathways)

to manage inflammation-related degeneration during spaceflight.

Metabolic remodeling and organelle dynamics

hBMSCs downregulated antioxidant defenses, cytosolic protein import, and fusion–fission dynamics, while osteocytes transiently increased outer-membrane translocase activity at day 4 but suppressed inner-membrane import at day 2. Glycolysis was upregulated in osteocytes at day 6, coupled with suppressed fatty-acid oxidation and an unaltered net mitochondrial metabolism score, whereas hBMSCs shifted toward increased glycolysis and decreased fatty-acid synthesis, with a downregulation of mitochondrial metabolism (Fig. 3). Mouse brain instead activated broad metabolic modules, including fatty-acid oxidation. Osteocytes also repressed the integrated stress response (ISR) at day 6 via loss of survival factors, while hBMSCs showed no net ISR change due to opposing downregulation of autophagy targets and upregulation of ISR regulators (Fig. 3). The UPR^MT/ER pathway was transiently downregulated in osteocytes at day 2 (via UPR-ER targets) and compensated thereafter, whereas hBMSCs displayed a compensatory upregulation (Fig. 3). mTOR signaling was inhibited in osteocytes at day 2, coherently with complex I suppression, and activated in hBMSCs through AMPK and REDD1 induction alongside GSK3β repression (the latter also occurring in osteocytes at day 6).

The alteration in mitochondrial import/export and stress responses may be early markers of microgravity-induced dysfunction. *SLC25A12* and *SLC25A20* (Figs. 2 and 3), involved in the mal/asp shuttle and carnitine/acylcarnitine transport respectively, are pivotal for maintaining mitochondrial membrane potential and were downregulated in hBMSCs, potentially impairing both energy production and antioxidant defenses. The induction of glycolysis in both hBMSCs and osteocytes likely reflects HIF-mediated compensation for impaired OXPHOS, in line with prior evidence of glycolytic reprogramming during mitochondrial stress [15, 16]. Modulation of mTOR and UPR^MT/ER pathways further support the idea that SLC25A-linked carrier defects initiate broader signaling changes. These pathways are attractive therapeutic targets to restore bioenergetics and proteostasis under spaceflight conditions.

Global reprogramming of MitoCarta pathways under microgravity

Transcriptomic signatures mapped to MitoCarta 3.0 functional modules revealed a tissue- and time-specific reorganization of mitochondrial physiology under microgravity conditions (Fig. 4).

Global trends

At 14 days, hBMSCs exhibited widespread downregulation (NES < 0, FDR < 0.3) across all MitoCarta modules except for a modest activation of pyruvate metabolism. Osteocytes showed minimal significant changes at 2 and 4 days, but by 6 days most pathways were downregulated, reflecting a coordinated suppression of mitochondrial functions, with a few exceptions related to the Metabolism module (OXPHOS, amino acid metabolism, cholesterol derivative biosynthesis, glyoxylate metabolism, NAD^+ biosynthesis, mitochondrial ribosome), most likely reflecting an attempt of the cell to counteract oxidative stress and mitochondrial dysfunction. In stark contrast, mouse brain at 84 days displayed widespread pathway activation (NES > 0) with the sole exceptions of mtDNA replication and sideroflexin-mediated small-molecule transport, which were observed downregulated.

These observations highlight the differential capacity of tissue types to cope with microgravity stress. The broad mitochondrial suppression observed in hBMSCs (14 days) and osteocytes (6 days) suggests an energy-conserving shutdown that may impair their regenerative roles, consistent with the observed loss of bone and muscle in microgravity conditions. In contrast, pathway activation in the brain likely reflects a neuroprotective adaptation to cosmic radiation exposure, enabled by enhanced carrier expression (e.g., *SLC25A10* (DIC)). The partial recovery observed in OXPHOS (CIII, CV, and assembly factors) and metabolic modules (CoA metabolism, detoxification, mal/asp shuttle, metals and cofactors, mitochondrial ribosome) in osteocytes at later timepoints suggests a window for therapeutic intervention aimed at key mitochondrial nodes. In particular, carriers implicated in early suppression, such as those involved in the mal/asp shuttle (*SLC25A11* (OGC), *SLC25A13* (AGC2)) and the uncoupling of oxidative phosphorylation (*SLC25A8* (UCP2)), represent potential targets, as they are functionally linked to mitochondrial diseases and energy homeostasis. (Table 1, Figs. 2 and 4). On the other hand, the downregulation of these same

carriers could serve as a biomarker for diagnosing tissue degeneration associated with microgravity conditions.

OXPHOS

hBMSCs at 14 days suffered significant downregulation of every OXPHOS submodule—assembly factors, complexes I–V and mitoribosome, consistent with earlier downregulation of mitochondrial carriers involved in direct interactions with respiratory chain complexes (i.e., *SLC25A12* (AGC1) participating to reducing equivalent exchange between mitochondria and cytosol through the mal/asp shuttle). Mouse brain robustly upregulated complexes I, III, and IV subunits and overall OXPHOS activity. Osteocytes presented a biphasic response, indeed complex I assembly factors were repressed at all timepoints; complexes I and III were significantly downregulated at 2 days and complex IV subunits decreased at 6 days. However, CIII assembly factors, complex V subunits and the mitoribosome were modestly upregulated by day 6, resulting in partial restoration of bioenergetic activity.

These findings reinforce the critical role of mitochondrial carriers in regulating OXPHOS integrity. The partial recovery of OXPHOS in osteocytes aligns with the upregulation of *SLC25A31* (AAC4), *SLC25A17* (CFNc or PMP34), *SLC25A22* (GC1), SLC25A36 (PNC2) at later stages. The strong OXPHOS upregulation in brain supports the resilience of neural mitochondria, possibly facilitated by sustained expression of dicarboxylate/phosphate transporters such as *SLC25A10* (DIC) (Table 1, Figs. 2 and 4). These carrier systems may serve as biomarkers of functional mitochondrial recovery or targets for countermeasure development in microgravity-exposed tissues.

Metabolism

Both hBMSCs (14 days) and osteocytes (6 days) repressed core metabolic pathways, including CoA and Fe–S biogenesis, metals. and cofactors, TCA cycle, type II fatty-acid synthesis, and vitamin metabolism, mirroring decreased carrier expression. Osteocytes at 6 days additionally downregulated biotin utilization, carnitine transport, choline/betaine, electron carriers, GABA, glutamate, glycine, iron homeostasis, phospholipids, other Q-linked reactions and the TCA cycle, while upregulating glyoxylate metabolism as well as NAD^+ biosynthesis, amino-acid metabolism, and cholesterol/bile-acid/steroid synthesis. In mouse brain, fatty-acid and amino-acid metabolism, CoA metabolism, malate–aspartate shuttle, detoxification, metals, cofactors, selenoproteins, and xenobiotic pathways were all significantly activated.

The downregulation of CoA and Fe–S cluster pathways indicates compromised electron flow, exacerbated by suppressed mitochondrial carriers involved in amino acid and organic acid transport. Altered amino-acid and vitamin metabolism links to suppressed *SLC25A12* (AGC1)/*SLC25A13* (AGC2), *SLC25A19* (TPC or DNC), *SLC25A16* (GDC, involved in CoA metabolism), which are also implicated in neurodevelopmental and metabolic disorders (Table 1, Figs. 2 and 4). These patterns highlight multiple SLC25A members, especially those linked to acylcarnitine, and amino acid flux, as potential targets for preserving metabolic flexibility in space-exposed tissues.

Central dogma

hBMSCs displayed a wholesale repression of mitochondrial protein synthesis and gene expression modules, with reference to mitoribosome assembly, mt-tRNA processing, mtDNA maintenance/replication, transcription, translation factors, RNA stability/decay, and polycistronic processing, consistently with the downregulation of mitochondrial carriers involved in amino acid metabolism (AGC1, HHH, SIDBA2, GC). Osteocytes at 6 days showed instead mitoribosome pathway activation alongside suppression of mtDNA repair/replication, transcription, and RNA metabolism; earlier (2–4 days) downregulation of mt-tRNA synthetases, translation, and transcription. Mouse brain remained largely unchanged in these modules except for a modest mtDNA replication decline.

This disconnection between transcriptional and translational modules suggests regulatory bottlenecks in mitochondrial gene expression. The downregulation of tRNA synthetases and translation factors in hBMSCs may reflect a programmed metabolic quiescence or response to carrier-linked deficits in amino acid exchange. In osteocytes, reactivation of ribosomal modules despite impaired DNA replication implies attempts to restore mitochondrial protein synthesis under stress. Carriers mediating nucleotide and antioxidant cofactors availability (e.g., *SLC25A36* (PNC2), *SLC25A6* (ANT3 or AAC3), *SLC25A40* (MCFP, involved in GSH/FeS metabolism) (Table 1, Figs. 2 and 4) or amino acid metabolism (AGC1, ORC1, CAC, GlyC, GC) could be central to these responses and represent therapeutic entry points for enhancing translation under compromised conditions.

Dynamics & surveillance

hBMSCs repressed cristae formation and MICOS complex modules. Osteocytes exhibited negligible changes at 4 days, a singular downregulation of organelle contact sites at 2 days, and by 6 days widespread inhibition of fusion, cristae, import contacts and surveillance—except for a late rebound in organelle contact-site modules. Brain dynamics and surveillance pathways were unaltered.

Suppressed dynamics and quality control mechanisms in hBMSCs and osteocytes align with a broader

mitochondrial dysfunction most likely responsible for tissue degeneration observed in microgravity conditions. Fusion/fission and contact site regulators are essential for stress adaptation, and their inhibition may result from or contribute to SLC25A-linked energy failure. The MICOS complex, critical for cristae structure and metabolite compartmentalization, could be indirectly affected by downregulation of inner membrane carriers such as those involved in amino acid metabolism or cofactor metabolism. This observation supports the therapeutic potential of targeting carrier-mediated flux to preserve cristae integrity and signaling.

Protein import, sorting & homeostasis

Both hBMSCs and osteocytes (2 and 6 days) downregulated TIM/TOM translocases, chaperones, proteases, and general import/sorting machinery. Osteocytes alone showed a transient TOM complex induction at 4 days. Brain cells displayed no significant changes in these modules.

These data suggest compromised protein import and folding as downstream consequences of mitochondrial depolarization or metabolite imbalance in osteocytes and hBMSCs, reflecting tissue degeneration observed in microgravity conditions, with reference to bone/muscle loss. The transient TOM activation in osteocytes may reflect early compensatory import of matrix enzymes or chaperones. The downregulation of the previously mentioned mitochondrial carriers (*SLC25A13* (AGC2), *SLC25A11* (OGC), and *SLC25A8* (UCP2) in osteocytes, or *SLC25A12* (AGC1), *SLC25A15* (ORC1), *SLC25A38* (GlyC)), *SLC25A22* (GC1), and *SLC25A30* (KMCP1 or UCP6), in hBMSCs) may also impact protein import by altering membrane potential, supporting their role as indirect regulators of proteostasis.

Signaling

Signaling pathways (calcium cycle, EF-hand proteins, immune response) were quiescent in hBMSCs and osteocytes until day 6, when osteocytes significantly repressed calcium-handling and immune-response modules. By contrast, mouse brain at 84 days mounted a strong activation of EF-hand and related signaling pathways.

Mitochondrial carriers (Table 1, Figs. 2 and 4) implicated in calcium homeostasis and linked to EF-hand signaling (with reference to *SLC25A12* (AGC1) and *SLC25A25* (APC1) in osteocytes, and *SLC25A10* (DIC) in brain) may mediate the observed alteration in signaling modules. Downregulation in osteocytes could impair Ca2±dependent stress responses or apoptosis regulation, while upregulation in brain could enhance neuroprotective signaling. These differences underscore the importance of tissue-specific carrier expression in shaping stress communication.

Small-molecule transport

hBMSCs and osteocytes at 6 days significantly repressed SLC25A carrier modules, reflecting the downregulation of multiple transporters; osteocytes also downregulated ABC transporters at 2–4 days. Mouse brain upregulated SLC25A carriers but suppressed sideroflexin pathways, underlining a divergent strategy of enhanced metabolite exchange in the CNS versus transport conservation in bone cells.

These patterns reinforce SLC25A members as central nodes of adaptation to spaceflight. hBMSCs and osteocytes reduce metabolite transport, most likely determining the observed tissue degeneration (with reference to bones and muscles) in microgravity conditions, while the brain prioritizes metabolite influx to support resilience. The upregulation of specific carriers, such as nucleotide carriers (*SLC25A31* (AAC4), *SLC25A36* (PNC2)), amino acid carriers (*SLC25A22* (GC1) and *SLC25A18* (GC2)), citrate carrier (*SLC25A1* (CIC)) or peroxisome CoA/FAD/NAD+ carrier (*SLC25A17* (CFNc or PMP34)) or the down regulation of *SLC25A13* (AGC2), *SLC25A11* (OGC) and *SLC25A8* (UCP2) in osteocytes, as well as amino acid carriers, cofactor carriers, and nucleotide carriers observed dysregulated in hBMSCs, emerge as markers of degeneration or adaptation, and may serve as reference targets for diagnosis screening or for intervention.

Global regulation of canonical signaling pathways by SLC25A modulation under microgravity

Hallmark Pathway analysis (via GSEA [40]) (Fig. 5) shows tissue- and time-dependent adaptation to microgravity.

Broad suppression of core regulatory pathways across tissues

GSEA done on the hallmark pathways from MSigDB further highlighted the systemic impact of spaceflight on cellular signaling, extending beyond mitochondrial processes and reflecting broader SLC25A-associated regulatory patterns across tissues (Fig. 5). Among the most consistent findings, the MYC Targets V1 and V2 pathways were downregulated across all timepoints in osteocytes, hBMSCs, and brain tissues, with the sole exception of MYC Targets V2 remaining unchanged in osteocytes at day 2. Similarly, Oxidative Phosphorylation was robustly suppressed in osteocytes and hBMSCs but significantly activated in brain tissue, mirroring mitochondrial pathway trends. A strong upregulation of the hypoxia pathway was observed at day 6 in osteocytes and hBMSCs, whereas it remained unaltered in brain tissue and at earlier osteocyte timepoints.

The consistent suppression of MYC target pathways across osteocytes, hBMSCs, and brain tissues, together with OXPHOS suppression in osteocytes and hBMSCs, indicates a shared core adaptation to microgravity

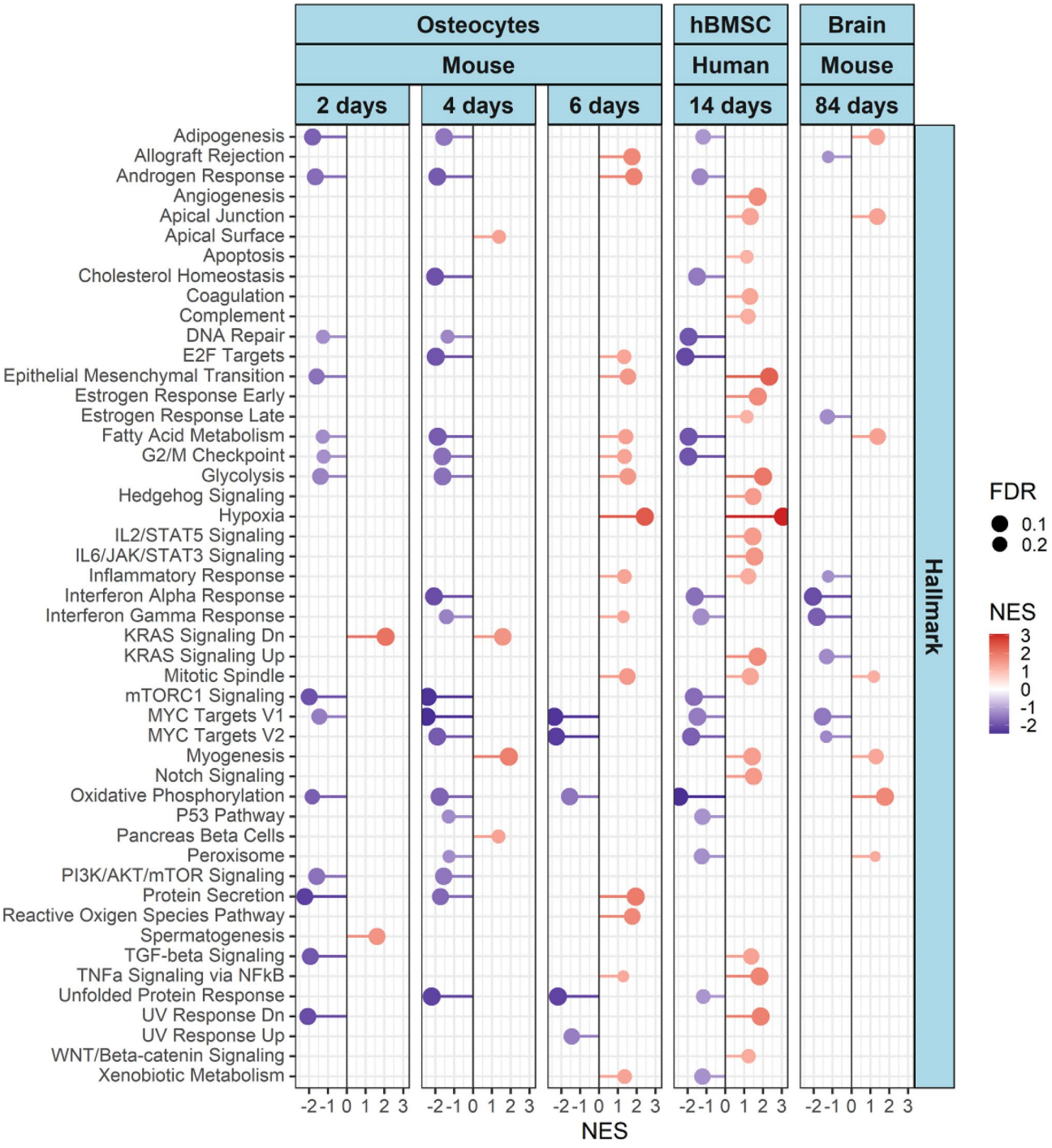

Fig. 5 Gene set enrichment analysis (GSEA) of hallmark pathways reveals tissue- and time-specific regulatory patterns associated with SLC25A activity. Pathway enrichment was assessed using hallmark gene sets from the MSigDB collection, which represent well-curated and biologically coherent processes (MSigDB hallmark collection). The normalized enrichment scores (NES) indicate the degree of upregulation (red) or downregulation (blue) for each pathway across osteocytes (mouse; 2, 4, and 6 days), hBmscs (human; 14 days), and brain (mouse; 84 days) under spaceflight conditions. Dot size reflects false discovery rate (FDR) significance, with larger dots corresponding to FDR < 0.1 and smaller dots to FDR < 0.2. The analysis highlights both conserved and divergent pathway regulation across tissues and timepoints, extending beyond mitochondrial signaling to include immune, metabolic, developmental, and stress-response pathways, underscoring the broad regulatory roles of SLC25A family members in microgravity adaptation

stress. This adaptation is characterized by reduced cell cycle progression driven by MYC suppression, particularly in muscles and bones (Fig. 5). Remarkably, whereas OXPHOS was suppressed in osteocytes and hBMSCs, it was enhanced in brain tissue, likely reflecting a compensatory neuroprotective response to microgravity-induced damage. The downregulation of MYC target pathways may synergize with the suppression of mitochondrial carriers in osteocytes, such as those involved in the mal/asp shuttle (*SLC25A13* (AGC2) and *SLC25A11* (OGC), contributing to redox homeostasis) and in membrane polarization maintenance and C4 metabolites exchange (*SLC25A8* (UCP2)). A similar pattern is evident in hBMSCs, where downregulation affects *SLC25A12* (AGC1) (mal/asp shuttle), *SLC25A15* (ORC1), *SLC25A22* (GC1) and *SLC25A38* (GlyC) (amino acid metabolism), *SLC25A16* (GDC, CoA metabolism), *SLC25A20* (CAC, carnitine shuttle and fatty acid oxidation), and *SLC25A30* (KMCP1 or UCP6, membrane polarization maintenance and C4 metabolite exchange). Collectively, these changes converge toward a systemic energy-conserving phenotype. This transcriptional program overlaps with hallmark pathways of oxidative phosphorylation, glycolysis, fatty acid metabolism, and reactive oxygen species response, consistent with a quiescent or stress-induced senescent state characteristic of tissue degeneration and cancer dormancy. Accordingly, the downregulated SLC25A carriers may not only serve as functional markers of metabolic suppression but also represent therapeutic entry points to preserve or restore mitochondrial output during spaceflight.

Temporal rebound of metabolic and cell cycle pathways in osteocytes

Osteocytes exhibited a dynamic temporal profile, with several pathways showing an initial downregulation at days 2 and 4 followed by a rebound at day 6. Specifically, Androgen Response, Fatty Acid Metabolism, G2/M Checkpoint, Glycolysis, and Protein Secretion became significantly upregulated by day 6. Meanwhile, Adipogenesis, DNA Repair, mTORC1 Signaling, and PI3K/AKT/mTOR Signaling recovered to baseline.

The rebound activation of metabolic and proliferative pathways at day 6 in osteocytes, including glycolysis and G2/M checkpoint signaling, reflects a late-phase adaptation or an attempt to adapt to microgravity. This suggests the engagement of compensatory bioenergetic circuits likely involving non-OXPHOS energy generation. The coordinated upregulation of mitochondrial carriers (*SLC25A1* (CIC), *SLC25A31* (AAC4), *SLC25A36* (PNC2), *SLC25A22* (GC1)) and the peroxisomal carrier *SLC25A17* (PMP34 or CFNc) likely reflects an adaptive attempt to counteract microgravity-induced stress. These transporters support distinct but complementary functions: *SLC25A1* (CIC) contributes to inflammation control, *SLC25A31* (AAC4, normally testis-specific) and *SLC25A36* (PNC2) sustain nucleotide metabolism and mitochondrial DNA biosynthesis, *SLC25A22* (GC1) fuels amino acid metabolism, and SLC25A17 (PMP34 or CFNc) facilitates cofactor and lipid metabolism. Collectively, their activity modulates inflammation, cofactor availability, and amino acid and fatty acid homeostasis, key processes in cellular recovery from microgravity stress or pre-hypertrophic states typically observed in muscle and bone. Such dynamics suggest a temporal window during which osteocytes acquire metabolic plasticity, and interventions that sustain or enhance the activity of these mitochondrial and peroxisomal carriers (Figs. 2 and 5) may help preserve osteoblast function and bone integrity during long-term spaceflight.

In hBMSCs, Adipogenesis and Fatty Acid Metabolism were repressed, while these same pathways were upregulated in brain tissue. Conversely, DNA Repair, Androgen Response, G2/M Checkpoint, and mTORC1 Signaling were downregulated in hBMSCs but remained unchanged in brain. Glycolysis was selectively induced in hBMSCs, whereas PI3K/AKT/mTOR Signaling and Protein Secretion stayed unaltered in both hBMSCs and brain.

The repression of Adipogenesis and Fatty Acid Metabolism in hBMSCs underscores a spaceflight-induced inhibition of lipid biosynthesis and energy storage, possibly reflecting metabolic stress or a shift toward survival over self-renewal. This transcriptional pattern aligns with reduced expression of fatty acid–related SLC25A members such as *SLC25A20* (CAC, carnitine shuttle, fatty acid oxidation). The selective suppression of DNA Repair, Androgen Response, G2/M Checkpoint, and mTORC1 Signaling, and MYC target pathways in hBMSCs points to impaired cell-cycle progression and reduced proliferative competence. This defect is likely reinforced by the downregulation of carriers mediating exchange of amino acids (*SLC25A12* (AGC1), *SLC25A15* (ORC1), *SLC25A38* (GlyC), *SLC25A22* (GC1)), cofactors (*SLC25A19* (DNC or TPC), *SLC25A25* (ATP-Mg/Pi), *SLC25A16* (GDC, proposed to be involved in CoA metabolism)), and fatty acid oxidation (*SLC25A20* (CAC)). At the same time, the induction of Glycolysis in hBMSCs may serve as a metabolic bypass to sustain ATP production under OXPHOS suppression. This shift is consistent with increased expression of nucleotide carriers *SLC25A6* (ANT3 or AAC3) and *SLC25A36* (PNC2). Remarkably, AAC3 has been linked to ATP uptake and uncoupling in pathological contexts [89, 96], while PNC2 supports mitochondrial DNA maintenance for reducing/counteracting apoptosis [71]. Remarkably, *SLC25A40*, proposed to function in GSH/Fe–S cluster metabolism and redox homeostasis,

was also upregulated, suggesting an additional layer of adaptation to oxidative stress.

By contrast, the relative stability or upregulation of these hallmark pathways in brain tissue highlights the resilience of the central nervous system to microgravity. This resilience is likely supported by carriers such as *SLC25A10* (DIC), which enhance organic dicarboxylates and phosphates shuttling, redox balance, contributing to mitochondrial DNA integrity, as previously observed [14]. Together, these divergent responses emphasize the role of SLC25A carriers as tissue-specific biomarkers and as pharmacologic entry points for modulating metabolic homeostasis under spaceflight conditions.

Immune and developmental pathway activation in hBmscs

An immune and developmental activation axis emerged prominently in hBMSCs. Robust upregulation was observed in Angiogenesis, Apoptosis, Coagulation, Complement, Estrogen Response Early, Hedgehog, IL2/STAT5, IL6/JAK/STAT3, Notch, and WNT/β-catenin signaling, none of which were altered in osteocytes or brain. Additionally, Estrogen Response Late showed mild elevation in hBMSCs and slight suppression in brain. The Inflammatory Response pathway increased in both osteocytes (day 6) and hBMSCs, while being suppressed in brain. KRAS Signaling Up was also activated in hBMSCs and repressed in brain.

The robust activation of immune and developmental pathways in hBMSCs, particularly IL/JAK/STAT, WNT, and Notch signaling, aligns with stem cell activation or stress-priming responses. Mitochondrial carriers such as *SLC25A20* (carnitine/acylcarnitine carrier) and *SLC25A38* (glycine carrier) (Figs. 2 and 5), both of which were downregulated in hBMSCs, have established roles in redox balance, apoptosis regulation, and hematopoietic cell maintenance. Their suppression may contribute to inflammatory signaling dysregulation and impaired erythropoiesis, echoing phenotypes seen in *SLC25A38*-linked congenital sideroblastic anemia. Given this, SLC25A modulation could be harnessed to buffer stem cell inflammation or prevent premature exhaustion, a key risk during long-term missions. Furthermore, *SLC25A17* (peroxisomal carrier (Figs. 2 and 5)) may indirectly influence immune lipid metabolism and deserves further study as a targetable node in hBMSC immunometabolic control.

Distinct and time-resolved responses in osteocytes and brain

Osteocyte-specific effects included Allograft Rejection pathway upregulation at day 6, transient boosts in Apical Surface and Pancreas Beta Cell pathways at day 4, and Spermatogenesis activation at day 2. The Cholesterol Homeostasis pathway was strongly repressed in hBMSCs and transiently downregulated in osteocytes at day 4. The E2F Targets module was suppressed in both osteocytes and hBMSCs at day 4 but slightly rebounded in osteocytes at day 6 (Fig. 5).

In osteocytes, the Epithelial–Mesenchymal Transition pathway was downregulated at day 2, returned to baseline at day 4, and became upregulated at day 6. In contrast, this pathway was strongly upregulated in hBMSCs and unchanged in brain.

Osteocyte-specific temporal changes, such as early upregulation of Spermatogenesis and later rebound of EMT and E2F targets, indicate a multiphasic transcriptional reprogramming reminiscent of tissue remodeling or stress-induced dedifferentiation. Downregulation of Cholesterol Homeostasis and ABC/SLC25A transporters (i.e., those involved in mal/asp shuttle (*SLC25A13* (AGC2) and *SLC25A11* (OGC)) involved in redox homeostasis and membrane polarization maintenance (*SLC25A8* (UCP2)) suggest impaired membrane and mitochondrial lipid trafficking, likely compromising vesicle dynamics and mitochondrial biogenesis. In brain tissue, the relative transcriptional stability across these axes underscores its resilience possibly aided by sustained *SLC25A10* upregulation and compensatory mtDNA repair activation. In osteocytes, the EMT rebound at day 6 could be linked to *SLC25A13* (AGC2) and *SLC25A22* (GC1) function aspartate/glutamate exchange, both critical for biosynthetic recovery under anabolic demand. These results raise the possibility of using *SLC25A10* (brain) and *SLC25A22* (bone) as markers or intervention targets for cell-specific mitochondrial stress responses (Figs. 2 and 5).

Immune signaling suppression and stress pathway rewiring

Interferon Alpha and Gamma Response pathways were downregulated in hBMSCs and brain tissues. Osteocytes displayed transient downregulation at day 4 followed by mild recovery at day 6. Selective activation of KRAS Signaling Down occurred in osteocytes at days 2 and 4.

Mitotic Spindle and Myogenesis were activated in all three tissues, while p53 and peroxisome pathways were downregulated in osteocytes and hBMSCs but upregulated in brain. The Reactive Oxygen Species pathway was activated in osteocytes at day 6, and TGF-β Signaling was suppressed early in osteocytes but upregulated in hBMSCs.

The general suppression of interferon pathways across tissues underlines a state of immune hypo-responsiveness, potentially reflecting mitochondrial damage-associated signaling blockade. MAVS pathway inhibition may contribute to impaired innate immune sensing and cytosolic mtDNA tolerance. The activation of Myogenesis and Mitotic Spindle pathways in parallel suggests a compensatory shift toward cytoskeletal remodeling and regeneration. In this context, targeting oxidative stress

regulators or supplementing cofactors for iron–sulfur biogenesis may enhance tissue resilience.

Given these alterations, pharmacologic inhibition of upregulated carriers such as *SLC25A1* (CIC), *SLC25A31* (AAC4), and *SLC25A36* (PNC2) in osteocytes, or *SLC25A6* (AAC3 or ANT3) and *SLC25A36* (PNC2) in hBMSCs, could help rebalance the excessive activation of glycolytic and nucleotide-supporting pathways. Conversely, stimulation of downregulated carriers such as *SLC25A13* (AGC2), *SLC25A11* (OGC), and *SLC25A20* (CAC) may restore mitochondrial function by reactivating lipid and redox metabolism in osteocytes and hBMSCs. Collectively, such targeted modulation of SLC25A carriers emerges as a rational strategy to counteract immune hypo-responsiveness, impaired DNA repair, and metabolic suppression under microgravity conditions.

Divergent regulation of stress and detoxification pathways

The strong activation of TNFα/NF-κB signaling in hBMSCs, and its moderate induction in osteocytes at later timepoints, reflects mounting inflammatory pressure. Because this pathway interacts with mitochondrial outer membrane proteins and regulates mitophagy, it raises interest in SLC25A-mediated control of inflammatory resolution (e.g., *SLC25A1* (CIC), upregulated in osteocytes). In parallel, the persistent repression of the Unfolded Protein Response (UPR^MT/ER) in osteocytes suggests chronic proteostasis stress and heightened vulnerability to misfolded protein accumulation. Alterations in UV response and xenobiotic metabolism further point to mitochondrial stress sensing and redox-dependent transcriptional tuning, particularly in hBMSCs. Taken together, these adaptations support the rationale for targeting mitochondrial stress modulators—either by inhibiting upregulated or stimulating downregulated SLC25A carriers—and/or enhancing chaperone and protease activity, as strategies to restore mitochondrial function and normalize mitochondria–cytosol cross-talk.

Structural modeling of mitochondrial carriers for drug design

Although only a few mitochondrial carrier (MC) proteins have been experimentally resolved, the availability of high-resolution crystallized structures of the AAC complexed with selective inhibitors provides a powerful foundation for comparative modeling of the entire MC family. These crystallized AAC structures, captured in both cytoplasmic-open (c-state, bound to CATR) and matrix-open (m-state, bound to BKA) conformations, enable the construction of accurate 3D models of human MCs [10, 12, 25]. Such models can be used to predict ligand-binding regions, evaluate structure–function relationships, and screen chemical libraries for novel molecules capable of modulating carrier activity, as previously demostrated for the human AAC2 and, more recently, for the human AGC2, also through in vitro binding/transport assays [10, 25].

Among all MCs, AACs represent ideal prototypes for this structural-based approach aiming to counteract the effects of microgravity and space-radiation. Beyond their canonical role in exchanging ADP and ATP across the inner mitochondrial membrane, AACs participate in mitochondrial apoptosis regulation that can be triggered or prevented by the administration of the two most famous AAC inhibitors (CATR and BKA [25, 89]). This dual regulatory potential makes AACs not only fundamental for cellular metabolism but also promising pharmacological targets for modulating apoptosis in different biological and environmental contexts [89, 96–98].

This approach is particularly relevant for space biology, as mitochondrial dysfunction and dysregulated apoptosis are hallmarks of cellular adaptation to microgravity and cosmic radiation [29, 31, 34]. In this setting, selective AAC modulators could serve to either enhance apoptosis in dysfunctional or hyperproliferative cells or suppress apoptosis to preserve bone and muscle mass, coherently with the upregulation of AAC3 observed in hBMSCs and the downregulation of AAC1 and AAC2 observed in osteocytes.

AAC3 modeling in c- and m-conformations

Based on these premises, we generated 3D comparative models of the human AAC3 in both the c- and m-conformations. The resulting AAC3 models displayed the typical six transmembrane α-helices expected for mitochondrial carriers, according to the existing crystallized structures and hydrophobic properties highlighted by multiple sequence alignments [2]. The backbone alignment between the modeled AAC3 and the respective templates yielded RMSD values below 0.2 Å (Fig. 6), confirming the structural accuracy of the comparative modeling process. These results are consistent with RMSD values obtained in our previous modeling of other MC members (typically < 0.6 Å), demonstrating the reliability of the method for capturing carrier topology and internal cavity geometry [2, 10, 12–17, 25–28, 51, 54, 72, 78, 93].

Re-docking and docking analysis of CATR and BKA within AAC3

To assess the reliability of the modeled AAC3 structures, a docking simulation was performed using the inhibitors CATR and BKA in the c- and m-conformations, respectively (Fig. 6). The gridboxes were defined according to those that best reproduced the crystallized BtAAC1–CATR and TtAAC1–BKA complexes, ensuring that all residues within 4 Å from the crystallized ligands were included in the binding regions to be explored.

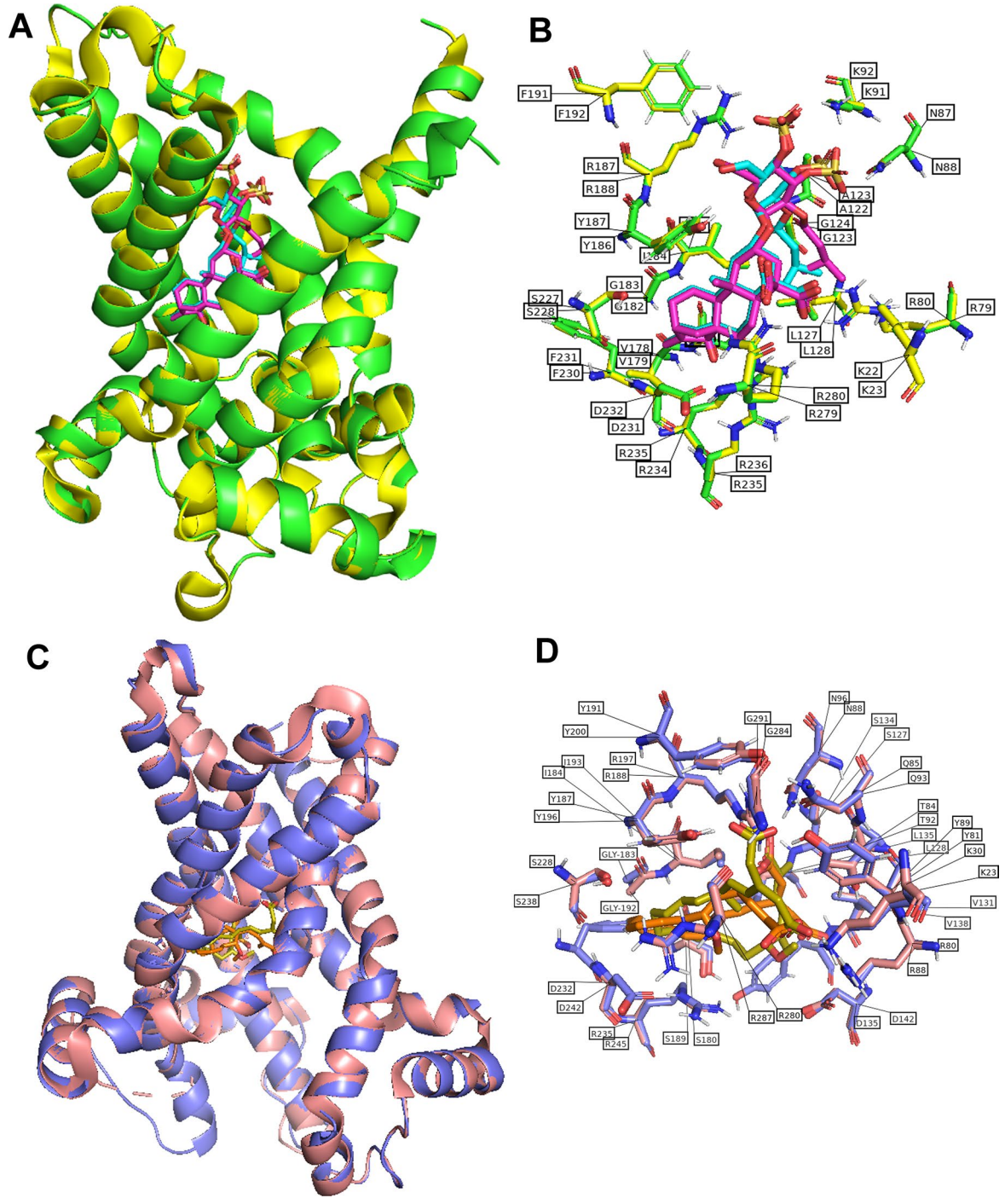

Fig. 6 Comparative structural analysis of human AAC3 with homologous ADP/ATP carriers in complex with inhibitors. (**a**) Superposition of the 3D comparative model of the human AAC3 (green cartoon) with the bovine BtAAC1 structure (yellow cartoon) crystallized in the *c*-conformation bound to CATR (magenta sticks). The docked CATR in human AAC3 is shown in blue sticks. (**b**) Zoomed view of residues within 4 Å from CATR in the *c*-conformation of AACs. Conserved interacting residues are labeled using the one-letter amino acid code, highlighting the strong structural conservation of the binding pocket residues. (**c**) Superposition of the 3D comparative model of the human AAC3 (pink cartoon) with the *Thermothelomyces thermophila* AAC1 (salmon cartoon) crystallized in the *m*-conformation bound to BKA (sand sticks). The docked BKA in human AAC3 is represented as orange sticks. (**d**) Zoomed view of residues within 4 Å from BKA in the *m*-conformation of AACs. Conserved interacting residues are indicated with boxed labels using the one-letter amino acid code, showing the high conservation of key interactions within the binding cavity

For both docking simulations, the ligand orientations closely matched those observed in the crystallized reference structures. The RMSD between the crystallized ligand poses and the docked conformations in the modeled AAC3 structures was below 0.8 Å for CATR and below 1.4 Å for BKA, indicating a good reproduction of experimentally observed binding geometries.

These findings validate the robustness of the modeling and docking pipeline. The accurate re-docking of CATR and BKA let us suppose that the generated AAC3 models can be reliably used for structure-based virtual screening of new ligands targeting either the c- or m-conformational states.

Implications for drug discovery and mitochondrial regulation

The good structural agreement between crystallized and re-docked complexes supports the broader use of this computational pipeline for the rational design and screening of small molecules capable of regulating mitochondrial carriers. In particular, it enables the identification of ligands (competing with ADP/ATP at the central binding site).

In this context, the recently reported AAC or AGC inhibitors such as chebulinic acid (for AAC), taurolithocholic acid 3-sulfate (for AGC) and suramin (for both AAC and AGC), predicted as AAC or AGC high affinity molecules through virtual screening of chemical libraries and validated through in vitro binding and transport assays, demonstrate the potential of the set-up combined in silico/in vitro pipeline [10, 25]. Suramin, an FDA-approved drug, exhibits six sulfonic groups arranged on aromatic rings, a configuration reminiscent of the sulfate-rich moieties of CATR. This structural similarity and the performed kinetics analysis suggest that suramin may selectively bind either the AAC or AGC in their c-conformations, acting as a competitive inhibitor. The possibility of repurposing such drugs to modulate AAC or AGC activity underscores the translational potential of this structural modeling approach. Finally, the validated docking workflow enables the identification of novel compounds that may regulate AAC (or AGC) function and, by extension, mitochondrial apoptosis, in physiological conditions and under environmental stressors such as microgravity or space radiation exposition.

Remarkably, the transcriptional and structural findings presented in this study provide a comprehensive view of how mitochondrial carrier modulation might contribute to cellular adaptation under spaceflight conditions and how structural knowledge can guide the identification of novel carrier modulators. At the transcriptional level, SLC25A family members, (i.e., with reference to *SLC25A6* (AAC3 also known as ANT3)), emerge as central mediators of metabolic flexibility, redox balance, and apoptotic control, particularly in osteocytes and hBMSCs. Structural modeling of AAC3 further highlights the potential to functionally modulate this carrier to mitigate the consequences of transcriptional dysregulation. The characterization of the existing AAC conformational states offers a framework for developing conformation-selective small molecules (pro-apoptotic or anti-apoptotic) capable of counteracting the energetic and oxidative imbalances induced by microgravity. The combination of the transcriptional/structural analysis underscores the translational relevance of SLC25A carriers as biomarkers of tissue vulnerability and as therapeutic entry points for the pharmacological restoration of mitochondrial function in spaceflights. Future work combining transcriptomic profiling with biochemical and structural validation of newly proposed ADP/ATP carrier high affinity small molecules, together with a multi-omics integration addressing the current lack of proteomic/metabolomic data, will be essential to confirm these adaptive mechanisms and to guide the rational design of mitochondrial-targeted therapeutics for long-term space missions.

Conclusion

This study provides a comprehensive, tissue-resolved analysis of the transcriptional regulation of SLC25A mitochondrial carriers under spaceflight conditions, revealing fundamental insights into the metabolic and signaling reprogramming that occurs in osteocytes, hBMSCs, and brain tissue during microgravity exposure. Our findings highlight that mitochondrial carriers, long regarded as passive facilitators of metabolite exchange, play a central and active role in coordinating bioenergetic, apoptotic, and immune responses across diverse cell types in response to mechanical unloading and space-induced stress.

Specifically, we observed the upregulation of *SLC25A6* (AAC3, also known as ANT3) in hBMSCs and *SLC25A31* (AAC4) in osteocytes, as well as the downregulation of *SLC25A8* (UCP2) in osteocytes and *SLC25A30* (KMCP1, also known as UCP6) in hBMSCs, most likely due to an attempt by the cell to stimulate OXPHOS and maintain mitochondrial membrane polarization. Notably, the upregulation of ADP/ATP carriers may be related to the proposed abilities of AACs to participate in mitochondrial respiration uncoupling or function as ATP importers [96, 97] when glycolytic pathways are upregulated, as it was observed in cases of partial mitochondrial impairment or membrane depolarization [15, 16]. This downregulation aligns with suppressed OXPHOS and may contribute to impaired stem cell renewal and osteogenic differentiation.

The concurrent repression in osteocytes and hBMSCs of *SLC25A12* (AGC1) and *SLC25A13* (AGC2, aspartate/glutamate antiporters), *SLC25A11* (OGC) involved in

Table 2 Summary of selected SLC25A mitochondrial carriers differentially regulated under spaceflight conditions

Gene (SLC25A)	Protein/Alias	Main Function	Spaceflight Response	Potential Use/Druggability
SLC25A6 (AAC3)	ADP/ATP Carrier 3	Nucleotide exchange, ATP turnover	Up in hBMSCs	Biomarker of compensatory energy metabolism; exploitable for inhibitor design
SLC25A31 (AAC4)	ADP/ATP Carrier 4	Nucleotide exchange (normally testis-specific)	Up in osteocytes	Stress-induced reprogramming marker, exploitable for inhibitor design
SLC25A36 (PNC2)	Pyrimidine Carrier 2	Pyrimidine/nucleotide metabolism	Up in osteocytes & hBMSCs	Biomarker for nucleotide stress; potential therapeutic target, exploitable for inhibitor design
SLC25A10 (DIC)	Dicarboxylate Carrier	Succinate/malate exchange	Up in brain	Neuroprotective adaptation marker, exploitable for inhibitor design
SLC25A12 (AGC1)	Aspartate/Glutamate Carrier 1	Mal/asp shuttle, redox balance	Down in hBMSCs	Marker of impaired respiration; targetable in cancer & metabolism, exploitable for agonist design
SLC25A13 (AGC2)	Aspartate/Glutamate Carrier 2	Mal/asp shuttle	Down in osteocytes	Biomarker of bone stress under microgravity, exploitable for agonist design
SLC25A15 (ORC1)	Ornithine Carrier 1	Urea cycle, amino acid metabolism	Down in hBMSCs	Marker of impaired nitrogen metabolism, exploitable for agonist design
SLC25A8 (UCP2)	Uncoupling Protein 2	Proton/C4 metabolite transport, ROS regulation	Down in osteocytes	Targetable for ROS modulation, biomarker of redox imbalance, exploitable for agonist design

the mal/asp shuttle ([9] with specific different features in AGC1 or AGC2 expression shown by osteocytes and hBMSCs), and *SLC25A20* (CAC, carnitine/acylcarnitine shuttle [12]) further points to a broad collapse of mitochondrial substrate flux, impairing redox balance and fatty acid metabolism. These molecular changes could underlie the propensity of the investigated tissues toward senescence, dedifferentiation, or aberrant lineage conversion, such as fibrotic trans-differentiation of myocytes or osteocytes under prolonged microgravity, causing bone and muscle loss [99]. This is supported by parallel suppression of MYC targets, DNA repair, and cell cycle regulators (e.g., G2/M checkpoint), as well as activation of hypoxia and inflammatory signaling, important for tissue regeneration and cell-cycle progression.

Conversely, in brain tissue, we observed a relative resilience characterized by the upregulation of *SLC25A10* (DIC, dicarboxylate carrier) and selective activation of OXPHOS subunits and mitochondrial quality-control modules. This suggests that CNS cells may sustain or even enhance mitochondrial capacity in long-duration space missions, possibly as a compensatory mechanism to resist oxidative damage and maintain neurotransmission. Indeed, *SLC25A10* (DIC) has already been linked to mitochondrial DNA maintenance [14]. Still, the downregulation of interferon responses and selective inflammatory rewiring raises concerns over immunometabolic fragility, particularly relevant to neurodegeneration in aged astronauts or during long-term missions.

The regulation of mitochondrial carrier expression was assessed at three different time points in osteocytes, showing a unique biphasic response with an early repression of key carriers and metabolic pathways, followed by a partial rebound as observed in glycolysis, UPRmt, and selected SLC25A genes (e.g., *SLC25A11* (OGC), *SLC25A13* (AGC2), and *SLC25A8* (UCP2)), implying a time-sensitive adaptation that may be leveraged for therapeutic priming or targeted interventions.

Taken together, our data strongly suggest that a subset of SLC25A mitochondrial carriers may serve dual roles as:

1. Diagnostic markers of tissue vulnerability to space-induced degeneration, with reference to the downregulation of *SLC25A4* (AAC1, also known as ANT1), *SLC25A5* (AAC2, also known as ANT2), *SLC25A24* (APC1) and the upregulation of *SLC25A1* (CIC), *SLC25A17* (PMP34 or CFNc), *SLC25A22* (GC1), *SLC25A31* (AAC4), *SLC25A36* (PNC2) in osteocytes at day 6, or the downregulation of *SLC25A20* (CAC), *SLC25A30* (KMCP1, also known as UCP6), *SLC25A12* (AGC1), *SLC25A15* (ORC1), *SLC25A16* (Grave's Disease carrier, also known as GDC, proposed to be involved in CoA metabolism), *SLC25A38* (Glyc), and the upregulation of *SLC25A6* (AAC3, also known as ANT3), *SLC25A40* (MCFP, involved in FeS cluster/GSH metabolism), and *SLC25A37* (MFRN1) in hBMSCs, or the upregulation of *SLC25A10* (DIC) in brain (Table 2).
2. Therapeutic targets for counteracting mitochondrial impairment, via small-molecule activation or stabilization of the mentioned carriers, particularly in bone and muscle tissues (Table 2).

Given their established roles in mitochondrial diseases and cancer metabolism on Earth [15, 16, 24], SLC25A family members provide a promising translational link between mitochondrial dysfunction and the pathophysiologic outcomes of spaceflight, such as skeletal unloading, myocyte–fibroblast transition, neuroinflammation, and stem cell depletion.

Future efforts should focus on pharmacological strategies to rescue the function or expression of these mitochondrial carriers and on evaluating their utility within biomarker-guided countermeasure programs. In this context, a gene expression panel of selected SLC25A carriers (like those mentioned above) could serve as a personalized diagnostic tool to predict individual vulnerability to microgravity-induced stress. Such panels could be integrated into astronaut health monitoring to enable earlier detection of preclinical mitochondrial dysfunction, reflecting a possible trigger of tissue degeneration.

In addition, the ability to accurately model mitochondrial carriers, such as AAC3, in both c- and m-conformations, and to reproduce their interactions with selective inhibitors (CATR and BKA, both active in vitro in the low-micromolar or nanomolar concentration range) at low/sub-angstrom (Å) precision, supports the use of structure-based computational approaches for drug discovery aimed at restoring mitochondrial homeostasis in spaceflight conditions or at least to reduce tissue degeneration by regulating mitochondrial apoptosis. In this regard, validated structural models and docking grid-boxes derived from the present study provide a robust computational framework for virtual screening and drug repurposing initiatives targeting mitochondrial carriers, particularly AACs, to modulate apoptosis and oxidative stress responses under microgravity.

These countermeasure programs may further benefit from combination approaches, including exercise, hypoxia mimetics, and, under extreme conditions, gene therapy or enzyme replacement strategies in cases of mitochondrial carrier loss. Incorporating carrier-dysregulation–based diagnostics and interventions into space health surveillance would represent a tangible step toward preserving astronaut musculoskeletal and cognitive integrity during long-term missions beyond Earth orbit. Although our approach is a bioinformatic/structural approach, the identification of druggable mitochondrial carriers opens new avenues for precision therapeutics. In particular, small-molecule or peptide modulators of AACs or AGCs could represent solid alternatives or adjuncts to current metabolic regulators [15, 16, 100]. Remarkably, recent studies exploring the cytotoxic and antimicrobial properties of plant- and marine-derived bioactive compounds [101, 102], together with the development of eco-sustainable nanocarrier systems for drug delivery [103, 104], highlight the translational importance of biologically compatible and sustainable materials for future space-flight health countermeasures. Beyond the mentioned biomedical implications, the expanding accessibility and accuracy of whole-genome sequencing, together with the growing availability of bioinformatic tools for comparative analysis and functional interpretation [105, 106] now make it feasible to identify and comparatively analyze mitochondrial carrier families across diverse biological taxa, including plants, fungi, and protists [17, 20–22]. Such comparative studies could illuminate evolutionarily conserved carrier adaptations that sustain life under extreme environmental pressures. For instance, radiotrophic fungi capable of metabolizing ionizing radiation [107, 108] may serve as natural models to explore how specific SLC25A-like transporters contribute to radiation tolerance and could be stimulated or engineered to enhance radiation adsorption in controlled orbital systems. Likewise, sequencing and expression profiling of deep-sea plant species thriving under high-pressure, hypoxic, and cold conditions, such as *Zostera marina* or extremophile algae, may guide the regulation of mitochondrial carrier expression in edible crops grown aboard space stations (e.g., *Solanum tuberosum* or *Lactuca sativa*). These cross-kingdom insights could inform the design of biologically resilient systems for food production and radiation protection in long-duration missions, thereby linking mitochondrial carrier biology to future life-support strategies beyond Earth orbit.

Acknowledgements
The authors would like to thank for the IT resources made available by ReCaS (https://www.recas-bari.it/index.php/en/), a project funded by the MIUR (Italian Ministry for Education, University and Research) in the "PON Ricerca e Competitività 2007–2013-Azione I-Interventi di rafforzamento strutturale" PONa3_00052, Avviso 254/Ric, University of Bari. In addition, the authors would like to thank the Italian Association for Mitochondrial Research – AIRM (http://www.mitoairm.it).

Author contributions
Conceptualization: Afshin Beheshti, Anna De Grassi, Pietro D'Addabbo, Ciro Leonardo Pierri. Data curation and formal analysis: Afshin Beheshti, Pietro D'Addabbo, Maria Noemi Sgobba, Anna Lucia Francavilla, Valeria Scaglione, Sabino Todisco, Ciro Leonardo Pierri. Supervision: Afshin Beheshti, Anna De Grassi, Lorenzo Guerra, Mariateresa Volpicella, Ciro Leonardo Pierri. Writing original draft: Pietro D'Addabbo, Anna De Grassi, Afshin Beheshti, Ciro Leonardo Pierri. Writing—review and editing: all the authors.

Funding
A.B. was supported by research funding from NASA E.9 Space Biology Research Studies 2023 grant. This research was also supported by EU funding within the MUR PNRR Extended Partnership initiative on Emerging Infectious Diseases (PE00000007, INF-ACT), MUR PNRR National Center for Gene Therapy and Drugs based on RNA Technology (CN_00000041), and PRIN 2022 PNRR - Next Generation EU Missione 4 Componente 1—CUP: H53D23008820001 (Project acronym "DI3DEM" cod. P2022N4CBF).

Data availability
The data that support the findings of this study are available from the corresponding author upon reasonable request. Data will be made available on request.

Declarations

Ethics approval and consent to participate
N/A.

Consent for publication
N/A.

Conflict of interest
The authors declare no conflicts of interest.

Author details
[1]Department of Biosciences, Biotechnologies and Environment, University of Bari "Aldo Moro", Via E. Orabona 4, 70125 Bari, Italy
[2]Center for Space Biomedicine, Mcgowan Institute for Regenerative Medicine, Department of Surgery, University of Pittsburgh, Pittsburgh, PA 15219, USA
[3]Stanley Center for Psychiatric Research, Broad Institute of MIT and Harvard, Cambridge, MA 02142, USA
[4]Laboratory of Biochemistry, Structural and Molecular Biology, Department of Pharmacy – Pharmaceutical Sciences, University of Bari "Aldo Moro", Via E. Orabona 4, 70125 Bari, Italy

Received: 15 October 2025 / Accepted: 20 November 2025
Published online: 30 December 2025

References

1. Palmieri F, Pierri CL. Mitochondrial metabolite transport. Brown G, Murphy M, editors. Essays Biochem. 47. 2010. p. 37–52.Available from: https://doi.org/10.1042/bse0470037
2. Pierri CL, Palmieri F, De Grassi A. Single-nucleotide evolution quantifies the importance of each site along the structure of mitochondrial carriers. Cell Mol Life Sci. 2014;71:349–64. Available from: https://doi.org/10.1007/s00018-013-1389-y
3. Palmieri F. The mitochondrial transporter family (SLC25): physiological and pathological implications. Pflugers Arch. 2004 [cited 2012 Jul 12];447:689–709. Available from: https://doi.org/10.1007/s00424-003-1099-7
4. Palmieri F, Pierri CL, De Grassi A, Nunes-Nesi A, Fernie AR. Evolution, structure and function of mitochondrial carriers: a review with new insights. Plant J. 2011 [cited 2012 Aug 23];66:161–81. Available from: https://doi.org/10.1111/j.1365-313x.2011.04516.x
5. De Grassi A, Lanave C, Saccone C. Evolution of ATP synthase subunit c and cytochrome c gene families in selected metazoan classes. Gene. 2006. https://doi.org/10.1016/j.gene.2005.11.022
6. Zheng J. Energy metabolism of cancer: glycolysis versus oxidative phosphorylation (review). Oncol Lett. 2012. https://doi.org/10.3892/ol.2012.928
7. Iacobazzi V, Infantino V. Citrate-new functions for an old metabolite. Biol Chem. 2014. https://doi.org/10.1515/hsz-2013-0271
8. TretterL, Adam-Vizi V. Inhibition of krebs cycle enzymes by hydrogen peroxide: a key role of α-ketoglutarate dehydrogenase in limiting NADH production under oxidative stress. J Neurosci. 2000;20:8972–79. https://doi.org/10.1523/jneurosci.20-24-08972.2000
9. Amoedo ND, Punzi G, Obre E, Lacombe D, De Grassi A, Pierri CL, et al. AGC1/2, the mitochondrial aspartate-glutamate carriers. Biochim Biophys Acta. 2016;1863:2394–412. Available from: https://doi.org/10.1016/j.bbamcr.2016.04.011
10. Cafferati Beltrame L, Todisco S, Francavilla AL, Mangini V, Bombino E, Sciancalepore AG, et al. Discovery of therapeutic AGC2 modulators by combining docking, binding, and vesicle-based transport assays. J Transl Med. 2025;23. https://doi.org/10.1186/s12967-025-07285-6
11. Infantino V, Pierri CL , Iacobazzi V. Metabolic routes in inflammation: the citrate pathway and its potential as therapeutic target. Curr Med Chem. 2018;26. https://doi.org/10.2174/0929867325666180510124558
12. Giangregorio N, Pierri CL, Tonazzi A, Incampo G, Tragni V, De Grassi A, et al. Proline/Glycine residues of the PG-levels guide conformational changes along the transport cycle in the mitochondrial carnitine/acylcarnitine carrier (SLC25A20). Int J Biol Macromol. 2022;221:1453–65. Available from: https://doi.org/10.1016/j.ijbiomac.2022.09.135.
13. Tessa A, Fiermonte G, Dionisi-Vici C, Paradies E, Baumgartner MR, Chien YH, et al. Identification of novel mutations in the SLC25A15 gene in hyperornithinemia-hyperammonemia-homocitrullinuria (HHH) syndrome: a clinical, molecular, and functional study. Hum Mutat. 2009 [cited 2012 Oct 2];30:741–48. Available from: https://doi.org/10.1002/humu.20930
14. Punzi G, Porcelli V, Ruggiu M, Hossain MF, Menga A, Scarcia P, et al. SLC25A10 biallelic mutations in intractable epileptic encephalopathy with complex I deficiency. Hum Mol Genet. 2018;27:499–504. Available from: https://doi.org/10.1093/hmg/ddx419
15. Todisco S, Musio B, Pesce V, Cavalluzzi MM, Petrosillo G, La Piana G, et al. Targeting mitochondrial impairment for the treatment of cardiovascular diseases: from hypertension to ischemia-reperfusion injury, searching for new pharmacological targets. Biochem Pharmacol. 2023. https://doi.org/10.1016/j.bcp.2022.115405
16. Tragni V, Primiano G, Tummolo A, Cafferati Beltrame L, La Piana G, Sgobba MN, et al. Personalized medicine in mitochondrial health and disease: molecular basis of therapeutic approaches based on nutritional supplements and their analogs. Molecules. 2022;27:3494. https://doi.org/10.3390/molecules27113494
17. Tragni V, Cotugno P, De Grassi A, Massari F, Di Ronzo F, Aresta AM, et al. Targeting mitochondrial metabolite transporters in penicillium expansum for reducing patulin production. Plant Physiol Biochem. 2020; https://doi.org/10.1016/j.plaphy.2020.07.027 . Available from: http://www.sciencedirect.com/science/article/pii/S0981942820303612
18. DeGrassi A, Lanave C, Saccone C. Genome duplication and gene-family evolution: the case of three OXPHOS gene families. Gene. 2008 [cited 2012 Aug 27];421:1–6. https://doi.org/10.1016/j.gene.2008.05.011. Available from: http://www.ncbi.nlm.nih.gov/pubmed/18573316
19. SacconeC, Lanave C, De Grassi A. Metazoan OXPHOS gene families: evolutionary forces at the level of mitochondrial and nuclear genomes. Biochim Biophys Acta. 2006 [cited 2012 Oct 2];1757:1171–78. https://doi.org/10.1016/j.bbabio.2006.04.021. Available from: http://www.ncbi.nlm.nih.gov/pubmed/16781661
20. Colasante C, Peña Diaz P, Clayton C, Voncken F. Mitochondrial carrier family inventory of trypanosoma brucei brucei: identification, expression and subcellular localisation. Mol Biochem Parasitol. 2009. https://doi.org/10.1016/j.molbiopara.2009.05.004
21. Nozawa A, Ito D, Ibrahim M, Santos HJ, Tsuboi T, Tozawa Y. Characterization of mitochondrial carrier proteins of malaria parasite Plasmodium falciparum based on in vitro translation and reconstitution. Parasitol Int. 2020 Dec;79:102160. PMID: 32574727. https://doi.org/10.1016/j.parint.2020.102160
22. Satre M, Mattei S, Aubry L, Gaudet P, Pelosi L, Brandolin G, et al. Mitochondrial carrier family: repertoire and peculiarities of the cellular slime mould Dictyostelium discoideum. Biochimie. 2007. https://doi.org/10.1016/j.biochi.2007.03.004
23. Palmieri F. Diseases caused by defects of mitochondrial carriers: a review. Biochim Biophys Acta. 2008 [cited 2012 Jul 13];1777:564–78. https://doi.org/10.1016/j.bbabio.2008.03.008. Available from: http://www.ncbi.nlm.nih.gov/pubmed/18406340
24. Palmieri F. The mitochondrial transporter family SLC25: identification, properties and physiopathology. Mol Asp Med. 2013;34:465–84. https://doi.org/10.1016/j.mam.2012.05.005. Available from: http://www.ncbi.nlm.nih.gov/pubmed/23266187
25. Todisco S, Di Noia MA, Onofrio A, Parisi G, Punzi G, Redavid G, et al. Identification of new highly selective inhibitors of the human ADP/ATP carriers by molecular docking and in vitro transport assays. Biochem Pharmacol. 2016;100:112–32. https://doi.org/10.1016/j.bcp.2015.11.019 . Available from: http://www.ncbi.nlm.nih.gov/pubmed/26616220
26. Palmieri EMM, Spera I, Menga A, Infantino V, Porcelli V, Iacobazzi V, et al. Acetylation of human mitochondrial citrate carrier modulates mitochondrial citrate/malate exchange activity to sustain NADPH production during macrophage activation. Biochim Biophys Acta. 2015;1847:729–38. https://doi.org/10.1016/j.bbabio.2015.04.009. Available from: http://www.ncbi.nlm.nih.gov/pubmed/25917893
27. Wibom R, Lasorsa FMFM, Töhönen V, Barbaro M, Sterky FHFH, Kucinski T, et al. AGC1 deficiency associated with global cerebral hypomyelination. N Engl J Med. 2009;361:489–95. Available from: https://doi.org/10.1056/nejmoa0900591
28. EdvardsonS, Porcelli V, Jalas C, Soiferman D, Kellner Y, Shaag A, et al. Agenesis of corpus callosum and optic nerve hypoplasia due to mutations in SLC25A1 encoding the mitochondrial citrate transporter. J Med Genet. 2013;50:240–45. https://doi.org/10.1136/jmedgenet-2012-101485. Available from: http://www.ncbi.nlm.nih.gov/pubmed/23393310
29. Waisberg E, Ong J, Masalkhi M, Mao XW, Beheshti A, Lee AG. Mitochondrial dysfunction in spaceflight associated neuro-ocular syndrome (SANS): a molecular hypothesis in pathogenesis. Eye. 2024. https://doi.org/10.1038/s41433-024-02951-3
30. Beheshti A, McDonald JT, Hada M, Takahashi A, Mason CE, Mognato M. Genomic changes driven by radiation-induced DNA damage and microgravity in human cells. Int J Mol Sci. 2021. https://doi.org/10.3390/ijms221910507
31. Camera A, Tabetah M, Castañeda V, Kim J, Galsinh AS, Haro-Vinueza A, et al. Aging and putative frailty biomarkers are altered by spaceflight. Sci Rep. 2024;14:13098. Available from: https://doi.org/10.1038/s41598-024-57948-5.

32. Ciofani G, Bandiera T, Corsini A, Crescenzi M, De Vittorio M, Mari S, et al. Pharmaceutical and biomedical challenges for crew autonomy in health preservation during future exploration missions. Commun Med. 2025;5:1–9. https://doi.org/10.1038/s43856-025-01128-7
33. Pashayev A, Garaybayli G, Mammadov A, Khalilov R, Eftekhari A. Biological insights from saliva diagnostics to assess human factors and flight safety performance in aviation simulators. Adv Biol Earth Sci. 2025. https://doi.org/10.62476/abes.102185
34. da Silveira WA, Fazelinia H, Rosenthal SB, Laiakis EC, Kim MS, Meydan C, et al. Comprehensive multi-omics analysis reveals mitochondrial stress as a central biological hub for spaceflight impact. Cell. 2020. https://doi.org/10.1016/j.cell.2020.11.002
35. Reno N, Initiative W, Prediction Q, Medicine WC, York N, Science C, et al. Guardians of the mitochondria: space mitochondria 2.0 systemic analysis reveals 2 bioenergetic dysregulation across species. 17–19. https://dx.doi.org/10.2139/ssrn.5087025
36. Overbey EG, Saravia-Butler AM, Zhang Z, Rathi KS, Fogle H, da Silveira WA, et al. NASA GeneLab RNA-seq consensus pipeline: standardized processing of short-read RNA-seq data. iScience. 2021. https://doi.org/10.1016/j.isci.2021.102361
37. Reimand J, Isserlin R, Voisin V, Kucera M, Tannus-Lopes C, Rostamianfar A, et al. Pathway enrichment analysis and visualization of omics data using g: profiler, GSEA, cytoscape and EnrichmentMap. Nat Protoc. 2019. https://doi.org/10.1038/s41596-018-0103-9
38. Korotkevich G, Sukhov V, Sergushichev A. Fgsea: fast gene set enrichment analysis. 2023. Available from: https://doi.org/10.1101/060012
39. Leyfer D, Fetterman JL. Beyond MitoCarta-expanding the list of candidate proteins involved in mitochondrial functions using a biological network approach. NAR Genomics Bioinforma. 2023. https://doi.org/10.1093/nargab/lqad107
40. Liberzon A, Birger C, Thorvaldsdóttir H, Ghandi M, Mesirov JP, Tamayo P. The molecular signatures database hallmark gene set collection. Cell Syst. 2015. https://doi.org/10.1016/j.cels.2015.12.004
41. Afshinnekoo E, Scott RT, MacKay MJ, Pariset E, Cekanaviciute E, Barker R, et al. Fundamental biological features of spaceflight: advancing the field to enable deep-space exploration. Cell. 2021. https://doi.org/10.1016/j.cell.2020.10.050
42. Kaplan RS, Mayor JA, Wood DO. The mitochondrial tricarboxylate transport protein: cDNA cloning, primary structure, and comparison with other mitochondrial transport proteins. J Biol Chem. 1993. https://pubmed.ncbi.nlm.nih.gov/8514800/
43. Porcelli V, Longo A, Palmieri L, Closs EI, Palmieri F. Asymmetric dimethylarginine is transported by the mitochondrial carrier SLC25A2. Amino Acids. 2016. https://doi.org/10.1007/s00726-015-2096-9
44. Fiermonte G, Dolce V, Palmieri F. Expression in Escherichia coli, functional characterization, and tissue distribution of isoforms A and B of the phosphate carrier from bovine mitochondria. J Biol Chem. 1998;273:22782–87. Available from: https://doi.org/10.1074/jbc.273.35.22782
45. Cimadamore-Werthein C, Jaiquel Baron S, King MS, Springett R, Kunji ER. Human mitochondrial ADP/ATP carrier SLC25A4 operates with a ping-pong kinetic mechanism. EMBO Rep. 2023. https://doi.org/10.15252/embr.202357127
46. Palmieri L, Alberio S, Pisano I, Lodi T, Meznaric-Petrusa M, Zidar J, et al. Complete loss-of-function of the heart/muscle-specific adenine nucleotide translocator is associated with mitochondrial myopathy and cardiomyopathy. Hum Mol Genet. 2005;14:3079–88. https://doi.org/10.1093/hmg/ddi341. Available from: http://www.ncbi.nlm.nih.gov/pubmed/16155110
47. Brüschweiler S, Yang Q, Run C, Chou JJ. Substrate-modulated ADP/ATP-transporter dynamics revealed by NMR relaxation dispersion. Nat Struct Mol Biol. 2015;22:636–41. https://doi.org/10.1038/nsmb.3059
48. Nicholls DG, Brand MD. A critical assessment of the role of creatine in brown adipose tissue thermogenesis. Nat Metab. 2023. https://doi.org/10.1038/s42255-022-00718-2
49. Vozza A, Parisi G, De Leonardis F, Lasorsa FM, Castegna A, Amorese D, et al. UCP2 transports C4 metabolites out of mitochondria, regulating glucose and glutamine oxidation. Proc Natl Acad Sci USA. 2014. https://doi.org/10.1073/pnas.1317400111
50. De Leonardis F, Ahmed A, Vozza A, Capobianco L, Riley CL, Barile SN, et al. Human mitochondrial uncoupling protein 3 functions as a metabolite transporter. FEBS Lett. 2024. https://doi.org/10.1002/1873-3468.14784
51. Spagnoletta A, Miniero DV, Gambacorta N, Oppedisano F, De Grassi A, Nicolotti O, et al. Modulatory effect of nicotinamide adenine dinucleotide phosphate (NADPH) on the 2-oxoglutarate mitochondrial carrier. Molecules. 2024;29:1–18. https://doi.org/10.3390/molecules29215154
52. Palmieri L, Pardo B, Lasorsa FM, Del Arco A, Kobayashi K, Iijima M, et al. Citrin and aralar1 are Ca2±stimulated aspartate/glutamate transporters in mitochondria. EMBO J. 2001;20:5060–69. https://doi.org/10.1093/emboj/20.18.5060
53. Curcio R, Muto L, Pierri CL, Montalto A, Lauria G, Onofrio A, Fiorillo M, Fiermonte G, Lunetti P, Vozza A, Capobianco L, Cappello AR, Dolce V. New insights about the structural rearrangements required for substrate translocation in the bovine mitochondrial oxoglutarate carrier. Biochim Biophys Acta. 2016 Nov;1864(11):1473-80. https://doi.org/10.1016/j.bbapap.2016.07.009 Epub 2016 Jul 30. PMID: 27479487
54. Fiermonte G, Parisi G, Martinelli D, De Leonardis F, Torre G, Pierri CL , et al. A new Caucasian case of neonatal intrahepatic cholestasis caused by citrin deficiency (NICCD): a clinical, molecular, and functional study. Mol Genet Metab. 2011;104:501–06. https://doi.org/10.1016/s0097-8485(96)80003-9. Available from: http://www.ncbi.nlm.nih.gov/pubmed/8867839
55. Gorgoglione R, Porcelli V, Santoro A, Daddabbo L, Vozza A, Monné M, et al. The human uncoupling proteins 5 and 6 (UCP5/SLC25A14 and UCP6/SLC25A30) transport sulfur oxyanions, phosphate and dicarboxylates. Biochim Biophys Acta - Bioenerg. 2019;1860:724–33. Available from: https://doi.org/10.1016/j.bbabio.2019.07.010
56. Fiermonte G, Dolce V, David L, Santorelli FM, Dionisi-Vici C, Palmieri F, et al. The mitochondrial ornithine transporter. Bacterial expression, reconstitution, functional characterization, and tissue distribution of two human isoforms. J Biol Chem. 2003;278:32778–83. Available from: https://doi.org/10.1074/jbc.M302317200
57. Prohl C, Pelzer W, Diekert K, Kmita H, Bedekovics T, Kispal G, et al. The yeast mitochondrial carrier Leu5p and its human homologue graves' disease protein are required for accumulation of coenzyme a in the matrix†. 2001;21:1089–97. Available from: file:///C:/Users/clpx/Documents/Mendeley-Library/Lindhurst. https://doi.org/10.1128/MCB.21.4.1089-1097.2001
58. Agrimi G, Russo A, Scarcia P, Palmieri F. The human gene SLC25A17 encodes a peroxisomal transporter of coenzyme a, FAD and NAD+. Biochem J. 2012;443:241–47. https://doi.org/10.1042/bj20111420. Available from: http://www.ncbi.nlm.nih.gov/pubmed/22185573
59. Agrimi G, Russo A, Pierri CL, Palmieri F. The peroxisomal NAD^+ carrier of Arabidopsis thaliana transports coenzyme a and its derivatives. J Bioenerg Biomembr. 2012;44. https://doi.org/10.1007/s10863-012-9445-0
60. Fiermonte G, Palmieri L, Todisco S, Agrimi G, Palmieri F, Walker JE. Identification of the mitochondrial glutamate transporter. Bacterial expression, reconstitution, functional characterization, and tissue distribution of two human isoforms. J Biol Chem. 2002;277:19289–94. Available from: https://doi.org/10.1074/jbc.m201572200
61. Lindhurst MJ, Fiermonte G, Song S, Struys E, De Leonardis F, Schwartzberg PL, et al. Knockout of Slc25a19 causes mitochondrial thiamine pyrophosphate depletion, embryonic lethality, CNS malformations, and anemia. Proc Natl Acad Sci USA. 2006;103:15927–32. Available from: https://doi.org/10.1073/pnas.0607661103
62. Fiermonte G, Dolce V, Palmieri L, Ventura M, Runswick MJ, Palmieri F, et al. Identification of the human mitochondrial oxodicarboxylate carrier. Bacterial expression, reconstitution, functional characterization, tissue distribution, and chromosomal location. J Biol Chem. 2001;276:8225–30. Available from: https://doi.org/10.1074/jbc.m009607200
63. Fiermonte G, De Leonardis F, Todisco S, Palmieri L, Lasorsa FM, Palmieri F. Identification of the mitochondrial ATP-Mg/Pi transporter. Bacterial expression, reconstitution, functional characterization, and tissue distribution. J Biol Chem. 2004;279:30722–30. Available from: https://doi.org/10.1074/jbc.m400445200
64. Agrimi G, Di Noia MA, Marobbio CMT, Fiermonte G, Lasorsa FM, Palmieri F. Identification of the human mitochondrial S-adenosylmethionine transporter: bacterial expression, reconstitution, functional characterization and tissue distribution. Biochem J. 2004;379:183–90. Available from: https://doi.org/10.1042/bj20031664
65. Lunetti P, Gorgoglione R, Curcio R, Marra F, Pignataro A, Vozza A, et al. Drosophila melanogaster uncoupling protein-4A (UCP4A) catalyzes a unidirectional transport of aspartate. Int J Mol Sci. 2022;23:1–16. https://doi.org/10.3390/ijms23031020
66. Han R, Liu L, Wang Y, Wu R, Yang Y, Zhao Y, et al. Microglial SLC25A28 deficiency ameliorates the brain injury after intracerebral hemorrhage in mice by restricting aerobic glycolysis. Inflammation. 2024. https://doi.org/10.1007/s10753-023-01931-1

67. Porcelli V, Fiermonte G, Longo A, Palmieri F. The human gene SLC25A29, of solute carrier family 25, encodes a mitochondrial transporter of basic amino acids. J Biol Chem. 2014;289:13374–84. Available from: https://doi.org/10.1074/jbc.m114.547448
68. Dolce V, Scarcia P, Iacopetta D, Palmieri F. A fourth ADP/ATP carrier isoform in man: identification, bacterial expression, functional characterization and tissue distribution. FEBS Lett. 2005;579:633–37. Available from: https://doi.org/10.1016/j.febslet.2004.12.034
69. Xue Z, Wang J, Wang Z, Liu J, Zhao J, Liu X, et al. SLC25A32 promotes malignant progression of glioblastoma by activating PI3K-AKT signaling pathway. BMC Cancer. 2023. https://doi.org/10.1186/s12885-023-11097-6
70. Santoro V, Kovalenko I, Vriens K, Christen S, Bernthaler A, Haegebarth A, et al. SLC25A32 sustains cancer cell proliferation by regulating flavin adenine nucleotide (FAD) metabolism. Oncotarget. 2020. https://doi.org/10.18632/oncotarget.27486
71. Di Noia MA, Todisco S, Cirigliano A, Rinaldi T, Agrimi G, Iacobazzi V, et al. The human SLC25A33 and SLC25A36 genes of solute carrier family 25 encode two mitochondrial pyrimidine nucleotide transporters. J Biol Chem. 2014;289:33137–48. Available from: https://doi.org/10.1074/jbc.m114.610808
72. Marobbio CMT, Giannuzzi G, Paradies E, Pierri CL, Palmieri F. Alpha-isopropylmalate, a leucine biosynthesis intermediate in yeast, is transported by the mitochondrial oxalacetate carrier. J Biol Chem. 2008;283:28445–53. Available from: https://doi.org/10.1074/jbc.m804637200
73. Seguin A, Jia X, Earl AM, Li L, Wallace J, Qiu A, et al. The mitochondrial metal transporters mitoferrin1 and mitoferrin2 are required for liver regeneration and cell proliferation in mice. J Biol Chem. 2020. https://doi.org/10.1074/jbc.ra120.013229
74. Lunetti P, Damiano F, De Benedetto G, Siculella L, Pennetta A, Muto L, et al. Characterization of human and yeast mitochondrial glycine carriers with implications for heme biosynthesis and anemia. J Biol Chem. 2016. https://doi.org/10.1074/jbc.m116.736876
75. Wang Y, Yen FS, Zhu XG, Timson RC, Weber R, Xing C, et al. SLC25A39 is necessary for mitochondrial glutathione import in mammalian cells. Nature. 2021. https://doi.org/10.1038/s41586-021-04025-w
76. Shi X, DeCiucis M, Grabinska KA, Kanyo J, Liu A, Lam TT, et al. Dual regulation of SLC25A39 by AFG3L2 and iron controls mitochondrial glutathione homeostasis. Mol Cell. 2024. https://doi.org/10.1016/j.molcel.2023.12.008
77. Fiermonte G, Paradies E, Todisco S, Marobbio CMT, Palmieri F. A novel member of solute carrier family 25 (SLC25A42) is a transporter of coenzyme a and adenosine 3',5'-diphosphate in human mitochondria. J Biol Chem. 2009;284:18152–59. Available from: https://doi.org/10.1074/jbc.m109.014118
78. Vozza A, De Leonardis F, Paradies E, De Grassi A, Pierri CL, Parisi G, et al. Biochemical characterization of a new mitochondrial transporter of dephosphocoenzyme a in Drosophila melanogaster. Biochim Biophys Acta. 2017;1858:137–46. Available from: https://doi.org/10.1016/j.bbabio.2016.11.006
79. Yoneshiro T, Wang Q, Tajima K, Matsushita M, Maki H, Igarashi K, et al. BCAA catabolism in brown fat controls energy homeostasis through SLC25A44. Nature. 2019;572:614–19. Available from: https://doi.org/10.1038/s41586-019-1503-x.
80. Steffen J, Vashisht AA, Wan J, Jen JC, Claypool SM, Wohlschlegel JA, et al. Rapid degradation of mutant SLC25A46 by the ubiquitin-proteasome system results in MFN1/2-mediated hyperfusion of mitochondria. Mol Biol Cell. 2017. https://doi.org/10.1091/mbc.e16-07-0545
81. Yook JS, Taxin ZH, Yuan B, Oikawa S, Auger C, Mutlu B, et al. The SLC25A47 locus controls gluconeogenesis and energy expenditure. Proc Natl Acad Sci USA. 2023. https://doi.org/10.1073/pnas.2216810120
82. Khan A, Unlu G, Lin P, Liu Y, Kilic E, Kenny TC, et al. Metabolic gene function discovery platform GeneMAP identifies SLC25A48 as necessary for mitochondrial choline import. Nat Genet. 2024;56:1614–23. Available from: https://doi.org/10.1038/s41588-024-01827-2.
83. Chen G, Mo S, Yuan D. Upregulation mitochondrial carrier 1 (MTCH1) is associated with cell proliferation, invasion, and migration of liver hepatocellular carcinoma. Biomed Res Int. 2021. https://doi.org/10.1155/2021/9911784
84. Chourasia S, Petucci C, Shoffler C, Abbasian D, Wang H, Han X, et al. MTCH2 controls energy demand and expenditure to fuel anabolism during adipogenesis. Embo J. 2025;44:1007–38. https://doi.org/10.1038/s44318-024-00335-7
85. Luongo TS, Eller JM, Lu MJ, Niere M, Raith F, Perry C, et al. SLC25A51 is a mammalian mitochondrial NAD+ transporter. Nature. 2020. https://doi.org/10.1038/s41586-020-2741-7
86. Girardi E, Agrimi G, Goldmann U, Fiume G, Lindinger S, Sedlyarov V, et al. Epistasis-driven identification of SLC25A51 as a regulator of human mitochondrial NAD import. Nat Commun. 2020. https://doi.org/10.1038/s41467-020-19871-x
87. Kory N, de Bos JU, van der Rijt S, Jankovic N, Güra M, Arp N, et al. MCART1/SLC25A51 is required for mitochondrial NAD transport. Sci Adv. 2020. https://doi.org/10.1126/sciadv.abe5310
88. Gong S, Zhai M, Shi J, Yu G, Lei Z, Shi Y, et al. TREM2 macrophage promotes cardiac repair in myocardial infarction by reprogramming metabolism via SLC25A53. Cell Death Differ. 2024. https://doi.org/10.1038/s41418-023-01252-8
89. Klingenberg M. The ADP and ATP transport in mitochondria and its carrier. Biochim Biophys Acta. 2008;1778:1978–2021. Available from: https://doi.org/10.1016/j.bbamem.2008.04.011
90. Pebay-PeyroulaE, Dahout-Gonzalez C, Kahn R, Trézéguet V, Lauquin G-M, Brandolin G. Structure of mitochondrial ADP/ATP carrier in complex with carboxyatractyloside. Nature. 2003;426:39–44. https://doi.org/10.1038/nature02056. Available from: http://www.ncbi.nlm.nih.gov/pubmed/14603310
91. Ruprecht JJ, Hellawell AM, Harding M, Crichton PG, McCoy AJ, Kunji ERS. Structures of yeast mitochondrial ADP/ATP carriers support a domain-based alternating-access transport mechanism. Proc Natl Acad Sci USA. 2014;111:E426–34. https://doi.org/10.1073/pnas.1320692111 . Available from: http://www.ncbi.nlm.nih.gov/pubmed/24474793
92. Ruprecht JJ, King MS, Zö T, Crichton PG, Steyaert J, Kunji ERS, et al. The molecular mechanism of transport by the mitochondrial ADP/ATP carrier correspondence the molecular mechanism of transport by the mitochondrial ADP/ATP carrier. Cell. 2019;176:435–47. Available from: https://doi.org/10.1016/j.cell.2018.11.025.
93. Giangregorio N, Tonazzi A, Pierri CL, Indiveri C. Insights into transient dimerisation of carnitine/acylcarnitine carrier (SLC25A20) from sarkosyl/PAGE, cross-linking reagents, and comparative modelling analysis. Biomolecules. 2024;14. https://doi.org/10.3390/biom14091158
94. Guarnieri JW, Dybas JM, Fazelinia H, Kim MS, Frere J, Zhang Y, et al. Core mitochondrial genes are down-regulated during SARS-CoV-2 infection of rodent and human hosts. Sci Transl Med. 2023 Aug 9;15(708):eabq1533. https://doi.org/10.1126/scitranslmed.abq1533 PMID: 37556555; PMCID:PMC11624572.
95. Rath S, Sharma R, Gupta R, Ast T, Chan C, Durham TJ, et al. MitoCarta3.0: an updated mitochondrial proteome now with sub-organelle localization and pathway annotations. Nucleic Acids Res. 2021. https://doi.org/10.1093/nar/gkaa1011
96. Le Bras M, Borgne-Sanchez A, Touat Z, El Dein OS, Deniaud A, Maillier E, et al. Chemosensitization by knockdown of adenine nucleotide translocase-2. Cancer Res. 2006;66:9143–52. Available from: https://doi.org/10.1158/0008-5472.can-05-4407
97. Trisolini L, Laera L, Favia M, Muscella A, Castegna A, Pesce V, et al. Differential expression of ADP/ATP carriers as a biomarker of metabolic remodeling and survival in kidney cancers. Biomolecules. 2021. https://doi.org/10.3390/biom11010038
98. Park D, Chiu J, Perrone GG, Dilda PJ, Hogg PJ. The tumour metabolism inhibitors GSAO and PENAO react with cysteines 57 and 257 of mitochondrial adenine nucleotide translocase. Cancer Cell Int. 2012;12:11. Available from: https://doi.org/10.1186/1475-2867-12-11
99. Juhl OJ, Buettmann EG, Friedman MA, et al. Update on the effects of microgravity on the musculoskeletal system. NPJ Microgravity. 2021;7:28. https://doi.org/10.1038/s41526-021-00158-4
100. Schmidt MA, Goodwin TJ. Personalized medicine in human space flight: using omics based analyses to develop individualized countermeasures that enhance astronaut safety and performance. Metabolomics. 2013. https://doi.org/10.1007/s11306-013-0556-3
101. Yaman U, Ince-Erguc E, Ozturk I, Okudan EŞ, Kirci D. Evaluation of cytotoxic and antimicrobial activities of methanolic extracts from Cystoseira foeniculacea and Sargassum vulgare. Adv Biol Earth Sci. 2025. https://doi.org/10.62476/abes.102347
102. El-Saadony MT, Saad AM, Mohammed DM, Korma SA, Alshahrani MY, Ahmed AE, et al. Medicinal plants: bioactive compounds, biological activities, combating multidrug-resistant microorganisms, and human health benefits - a comprehensive review. Front Immunol. 2025;16:1–37. https://doi.org/10.3389/fimmu.2025.1491777
103. Doğan Y, Öziç C, Ertaş E, Baran A, Rosic G, Selakovic D, et al. Activated carbon-coated iron oxide magnetic nanocomposite (IONPs@CtAC) loaded with morin hydrate for drug-delivery applications. Front Chem. 2024;12:1–10. https://doi.org/10.3389/fchem.2024.1477724

104. Öziç C, Ertaş E, Baran MF, Baran A, Ahmadian E, Eftekhari A, et al. Synthesis and characterization of activated carbon-supported magnetic nanocomposite (MNPs-OLAC) obtained from okra leaves as a nanocarrier for targeted delivery of morin hydrate. Front Pharmacol. 2024;15:1–9. https://doi.org/10.3389/fphar.2024.1482130
105. De Grassi A, Segala C, Iannelli F, Volorio S, Bertario L, Radice P, et al. Ultradeep sequencing of a human ultraconserved region reveals somatic and constitutional genomic instability. PLoS Biol. 2010. https://doi.org/10.1371/journal.pbio.1000275
106. Chander AM, Singh NK, Simpson AC, Seuylemezian A, Mason CE, Venkateswaran K. Draft genome sequences of fungi isolated from mars 2020 spacecraft assembly facilities. Microbiol Resour Announc. 2022. https://doi.org/10.1128/mra.00464-22
107. Averesch NJH, Shunk GK, Kern C. Cultivation of the dematiaceous fungus cladosporium sphaerospermum aboard the international space station and effects of ionizing radiation. Front Microbiol. 2022. https://doi.org/10.3389/fmicb.2022.877625
108. Bland J, Gribble LA, Hamel MC, Wright JB, Moormann G, Bachand M, et al. Evaluating changes in growth and pigmentation of Cladosporium cladosporioides and Paecilomyces variotii in response to gamma and ultraviolet irradiation. Sci Rep. 2022. https://doi.org/10.1038/s41598-022-16063-z

Publisher's Note